INVESTIGATION OF BRAIN ACTIVITY IN PREFRONTAL CORTEXUNDER NOXIOUS PAIN STIMULI AND DURING PSYCHOLOGICAL TEST USING FUNCTIONAL NEAR INFRARED SPECTROSCOPY

by

SABIN KHADKA

Presented to the Faculty of the Graduate School of

The University of Texas at Arlington in Partial Fulfillment

of the Requirements

for the Degree of

MASTER OF SCIENCE IN BIOMEDICAL ENGINEERING

THE UNIVERSITY OF TEXAS AT ARLINGTON

May 2011

ACKNOWLEDGEMENTS

First and foremost, I would like to thank my mentor Dr. Hanli Liu from the bottom of my heart for providing me an opportunity to work under her. Her constant supervision and guidance helped me in better understanding of problems and way to solve them. Her approach towards work, advice and suggestions has made a huge impact on me, which would help me on my future endeavors.

I would like to thank Dr. Georgios Alexandrikas for teaching me the fundamentals of tissue optics. Also, I thank him for being a committee member and helping me better with my thesis. My sincere thanks go to Dr. Baohong Yuan for accepting to be a committee member.

It gives me a pleasure to thank Dr. Fenghua Tian and Dr. Haijing Niu for helping me a lot in better understanding the technical aspects of my work. A very special thank goes to Dr. Nancy Rowe for her guidance and advices with statistical analysis during my project. I would like to thank Mr. Zi-jing Lin and Mr. Vikrant Sharma for their suggestions and input throughout my project. Also, I would like to thank Ms. Pamela A. Tebebi for building the pain generator that I used for my thesis research. I would also like to thank Mr.Pritam Gautam and Mr. Srujan Reddy Chityala for helping me with experiments and data acquisition. A healthy environment at work is a must, thus I would like to take this opportunity to acknowledge all of my lab members whose constant support, encouragement and advices were valuable to me.

Last but not the least, my sincere gratitude and thankfulness go to my parents and brothers whose constant love and support have been a source of encouragement for me.

April 22, 2011

ABSTRACT

INVESTIGATION OF BRAIN ACTIVITY IN PREFRONTAL CORTEX UNDER NOXIOUS PAIN STIMULI AND DURING PSYCHOLOGICAL TESTUSING FUNCTIONAL NEAR INFRARED SPECTROSCOPY

Sabin Khadka, M.S.

The University of Texas at Arlington, 2011

Supervising Professor: Hanli Liu

Functional Near Infrared Spectroscopy (fNIRS) is a non-invasive functional neuroimaging technique, which measures changes in oxy-hemoglobin (HbO) and deoxy-hemoglobin (HbR) concentrations based on the principle of near infrared spectroscopy. For my thesis, I have utilized fNIRS in the prefrontal regions to study cognitive functions under noxious pain and during a psychological test.

The fNIRS signals were acquired from the prefrontal cortex (PFC) in order to investigate the hemodynamic response under noxious pain stimuli. The measurement consisted of two different visits separated by seven to ten days with two different levels of pain intensity. From the observations, PFC shows significant deactivation in response to higher noxious pain stimuli. Also, I observed that the temporal HbO profiles in contra-lateral PFC show significant differences in response to two pain stimuli. The response of HbO in medial anterior prefrontal cortex exhibits a better correlation with the behavioral pain rating in response to higher pain stimuli. The results reveal that the fNIRS is able to detect the hemodynamic activities in

response to noxious pain stimuli and can be a potential neural correlate for cognitive evaluation of pain.

In the second part of study, fNIRS signals were acquired from anterior prefrontal cortex (aPFC) in order to investigate the hemodynamic activity while performing a psychological test. A psychological test, called Stroop test, was used to investigate the activity in aPFC. Stroop test is a commonly used to investigate the attention and cognitive control of the brain. The fNIRS results have shown detectable activities in aPFC while performing the Stroop test. Also, as the difficulty of task increases or more attention is required, the changes in HbO are higher in right aPFC. Thus, the change in HbO in aPFC may be a potential neural correlate for human cognitive functions.

TABLE OF CONTENTS

LIST OF ILLUSTRATIONS

CHAPTER 1

INTRODUCTION

1.1 Principle of Near Infrared Spectroscopy

1.1.1 Functional Near Infrared Spectroscopy

Functional Near Infrared Spectroscopy (fNIRS) is a well known non-invasive imaging modality which is used to detect neural activation in human brain. This technique utilizes interaction of light in near-infrared wavelength with biological tissues that is mainly due to the process of absorption and elastic scattering. The wavelength of near-infrared light is in the range of 650 nm to 950 nm which is slightly beyond the visible light, as shown in fig. 1.1. Different physiological chromophore molecules including oxy-hemoglobin (HbO or oxyHb) and deoxy-hemoglobin (HbR or deoxyHb) have unique absorption spectra in the near infrared wavelength region.

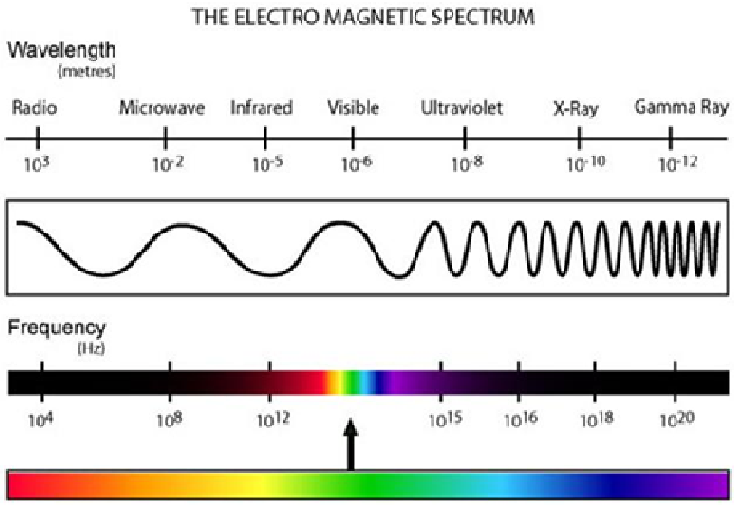

Figure 1.1 Electromagnetic spectrum[40]

Change in HbO and HbR concentration can act as an indicator of blood volume and oxygenation in tissue of interest[1]. The interaction between light and biological tissues can be defined by two parameters: absorption coefficient, μa, and reduced scattering coefficient, μs'. μa is defined as the number of absorption events occurring per unit length, whereas μs' is the number of scattering events occurring per unit length. μa contains most of the hemodynamic information; however, μs' is considerably larger in tissue, due to which the signals measured at a few millimeters or larger are dominated by the diffuse light.

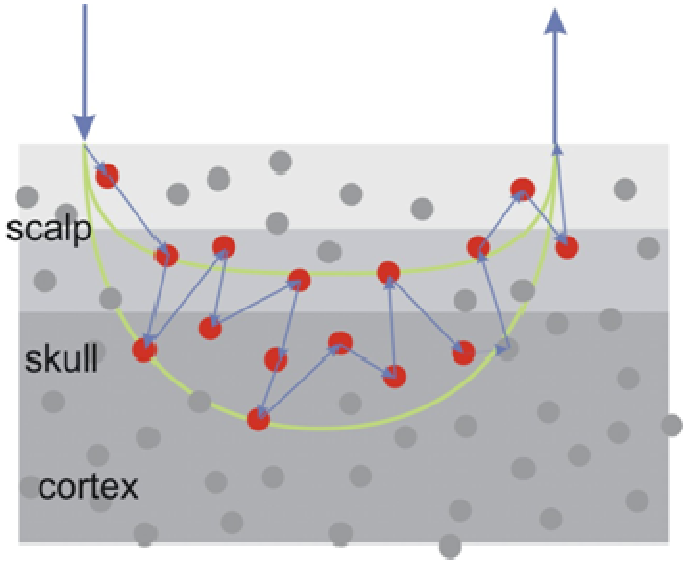

Figure 1.2 Banana-shaped pattern of photons in scalp [41]

Various physiological monitoring techniques, such as pulse oximetry and near-infrared spectroscopy (NIRS), take advantage of different absorption spectra of HbO and HbR. fNIRS is a spectroscopic method and capable of non-invasively measuring changes in concentration of HbO and HbR using near infrared light. fNIRS-based brain imaging method makes use of spatially distributed and interlaced source-detector pairs with overlapping measurement volumes to detect absorption change of HbO and HbR. The photons in the brain follow the banana-shaped pattern between the source and detector, as shown in fig. 1.2. The goal of this technique is to produce spatially resolved images. These images may display the specific

absorption and scattering properties of the tissue, or physiological parameters, such as blood volume and oxygenation or HbO and HbR concentrations [2]. To be able to filter undesired physiological artifacts, fNIRS techniques require a faster sampling rate. Also, it is better to cover large brain areas, extending beyond the area involved with stimulation, which will help get a contrast between the area of activation and surrounding [3].

1.1.2 Optical window

The operating wavelength of fNIRS is in the range of around 670 nm to 950 nm. The characteristic absorption spectra ("spectroscopic fingerprints") are different for HbO and HbR molecules. HbO, HbR and water are dominant absorbers in the visible and near infrared wavelengths. The characteristic absorption spectra of HbO and HbR are shown in fig. 1.2.

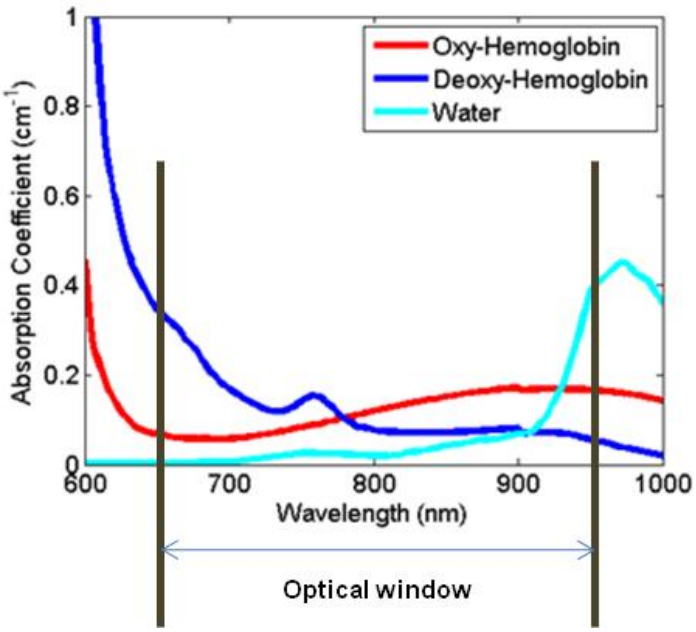

Figure 1.3 Absorption spectra of Oxy-hemoglobin, Deoxy-hemoglobin and water [42]

Light in the visible wavelength range is strongly absorbed by hemoglobin; also at wavelengths longer than 950 nm, the light absorption due to water is very high. Relatively, in the near infrared range between 650 nm to 950 nm, the absorption of light due to HbO, HbR and water is relatively low; thus, this spectral range is relatively transparent for most biological tissues and is called “optical window”(see fig. 1.3). Using multiple wavelengths within the “optical window”, changes in HbO, HbR and total Hemoglobin (HbT) can be measured simultaneously[28].

1.1.3 Modified Beer-Lambert Law

In fNIRS, near infrared light diffuses through the scalp and skull of the human head, which causes changes in optical density (ΔOD) due to absorption[4]. This ΔOD is assumed to be small and can be modeled as a linear combination of changes in HbO and HbR, following the modified Beer-Lambert law (MBLL) (5,6). The change in concentration (and thus in absorbing coefficient) causes the detected light intensity to change as well. According the MBLL, change in concentration can be related to ΔOD by equation (1.1)

$$\Delta OD = \log (I_o/I) = \varepsilon c L = kc \quad \text{..... (1.1)}$$

Where

ΔOD = change in optical density,

I_o = Light intensity before the change of concentration,

I = Light intensity after the change of concentration,

ε = extinction coefficient of absorbing tissue,

L = path length through the tissue,

k = proportionality constant.

The path length that the scattered light actually traveled through the tissue can be decomposed into source-detector separation (d) and the differential path length (DPF), L = d * DPF. The source-detector separation can be known from the probe geometry design, whereas DPF is either measured with a time-domain or frequency domain instrument or estimated using a continuous wave measurement. The proportionality constant, k, contains extinction coefficient which could be looked up in the literature and the path length of the scattered light travelled through the tissues, k = ε * L.

The contributions of multiple chromophores, such as HbO and HbR, can be determined by talking the measurements at one or more wavelengths per chromophore to be resolved. By measuring ΔOD at two wavelengths and using the known extinction coefficients of HbO (εHbO) and HbR (εHbR) at wavelengths within the optical window (refer to section1.1.2), the concentration changes of HbO and HbR can be separately determined by solving the following equations (1.2) , (1.3) and (1.4) [7]:

$$\Delta[\mathrm{HbO}] = \frac{\varepsilon\mathrm{HbR}^{\lambda 2} * \mathrm{OD}^{\lambda 1} - \varepsilon\mathrm{HbR}^{\lambda 1} * \mathrm{OD}^{\lambda 2}}{\mathrm{L} * (\varepsilon\mathrm{HbR}^{\lambda 2} * \varepsilon\mathrm{HbO}^{\lambda 1} - \varepsilon\mathrm{HbR}^{\lambda 1} * \varepsilon\mathrm{HbO}^{\lambda 2})} \quad \ldots\ldots 1.2$$

$$\Delta[\mathrm{HbR}] = \frac{\varepsilon\mathrm{HbO}^{\lambda 2} * \mathrm{OD}^{\lambda 1} - \varepsilon\mathrm{HbO}^{\lambda 1} * \mathrm{OD}^{\lambda 2}}{\mathrm{L} * (\varepsilon\mathrm{HbR}^{\lambda 1} * \varepsilon\mathrm{HbO}^{\lambda 2} - \varepsilon\mathrm{HbR}^{\lambda 2} * \varepsilon\mathrm{HbO}^{\lambda 1})} \quad \ldots\ldots 1.3$$

$$\Delta[\mathrm{HbT}] = \Delta[\mathrm{HbO}] + \Delta[\mathrm{HbR}] \quad \ldots\ldots 1.4$$

1.2 Brain Physiology

The fundamental goal of functional imaging is to create images of physiological activities which correlate with neuronal activity. Human brain undergoes many physiological changes in response to the external stimuli. Activity in neurons due to the physiological change increases their metabolic requirements. Thus, there is an influx of oxygenated blood into these areas which causes changes in concentration of HbO and HbR. The change in concentration of HbO and HbR can be detected by the fNIRS technique by detecting the changes in absorption of near infrared light[8].

1.2.1 Neurovascular coupling

Neurovascular coupling refers to the relationship between neuronal activity and the associated cerebral blood flow (which causes hemodynamic changes). Since fNIRS study deals with measurement of hemodynamic changes in the brain due to some external stimuli, a very good understanding of this phenomenon is required for interpretation of functional imaging data and normal brain function.

Neurovascular coupling is caused by the interaction between neurons, glia, and vascular cells. The neuronal chemo-electrical activity is associated with several metabolic cascades, which is also known as neurovascular coupling. Glucose is metabolized to lactate in astrocytes by anaerobic glycolysis. The lactate is then utilized by the neurons and metabolized with oxygen forming ATP and carbon dioxide. From surrounding capillaries, HbO is delivered to the neurons and releases its oxygen in the presence of carbon dioxide, thus converting HbO into HbR. The vasoactive factors released in response to neurotransmitter can be a cause of vasodilation, such as activation of glutamate receptors. Here, the intracellular Ca^{2+} of astrocytes associated with glutamate receptor activation causes Ca^{2+}-dependent enzymes to produce vasodilators, such as nitric oxide (NO).

The extracellular ionic currents caused by action potential and synaptic transmissions generate ions K^+ and H^+, causing increase in blood flow and volume and causing smooth muscles in the arterioles to hyperpolarize and relax. Also, increase in blood flow can be caused by release in neurotransmitter, such as acetocholine causing the smooth muscles arterioles to relax[15, 38].

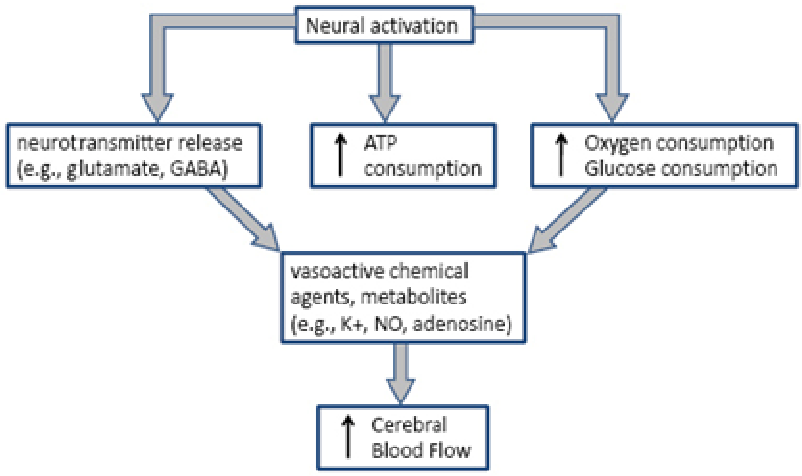

Figure 1.4 Neurovascular coupling[39]

Brain activity is associated with a number of physiological events and is summarized in fig. 1.4. Since neuronal activation is fueled by glucose metabolism, an increase in neuronal activity increases the consumption of glucose and oxygen. However, reduction of glucose and oxygen in the capillaries stimulates the brain to increase local arteriolar vasodilation. The dilation of arteries leads to an increase of local cerebral blood flow and cerebral blood volume.

1.2.2 Prefrontal Cortex

The prefrontal cortex (PFC) in the cerebral cortex is located just anterior to the motor and premotor areas (see fig. 1.5). This region is mainly involved in cognitive control, planning, personality expression and decision making[9 , 10]. PFC is mainly involved in cognitive control and executive function. Executive function can be defined as the ability of one to differentiate between various conditions.

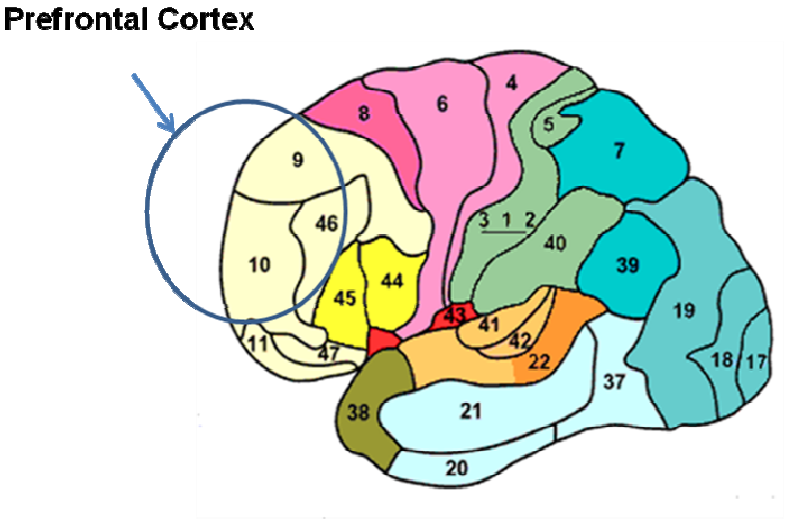

Figure 1.5 Broadmann area of the brain [56]

1.2.2.1 Dorsolateral Prefrontal Cortex

The dorsolateral prefrontal cortex (DLPFC) is a part of PFC represented by Broadmann areas 9 and 46 in fig. 1.5. The DLPFC is one of the most interconnected regions of the association cortices. DLPFC is connected to various cortical and subcortical regions of the brain. DLPFC is known as the highest cortical area which is responsible for motor planning, regulation and organization. Also, it plays an important role in working memory.

1.2.2.2 Anterior Prefrontal Cortex

The anterior prefrontal cortex (aPFC) is a part of PFC represented by Broadmann area 10 shown in fig. 1.5. aPFC covers a large area in the human brain; however, it is described as "one of the least well understood regions in the human brain" [11]. This region is responsible for the executive function of the human brain. The larger size of aPFC in humans as compared to other primates and its development in humans in later stage of the life suggests the role of aPFC in cognition. Also, it is suggested that aPFC is responsible for self generating information and involved in solving complex problems[16,17]. Various functional neuroimaging studies have reported activities in aPFC while performing cognitive trials [12-15].

1.3 Pain

1.3.1 Perception of Pain

According to the International Association for the Study of Pain (IASP), pain is defined as "an unpleasant sensory and emotional experience associated with actual or potential tissue damage, or described in terms of such damage" [59]. Even though the pain is mediated by the nervous system, a distinction between pain and neural mechanisms of nociception -the response to perceived or actual tissue damage- is important both clinically and experimentally. Nociceptors, which are specialized sensory receptors, are activated by noxious insults to peripheral tissues. However, nociception does not necessarily lead to the experience of pain[18].

1.3.2 Classification of Pain

Pain can be classified in two categories: temporal or physiological. When pain is classified by time depending upon the duration of pain, it is defined either as acute or chronic. Acute pain lasts for a short duration and has an identifiable pathology, whereas chronic pain

lasts for a period that extends beyond an expected period of healing and has unclear pathology[18-20].

Pain can also be classified into nociceptive pain and neuropathic pain. Nociceptive pain results from the direct activation of nociceptors in the skin or soft tissue in response to tissue injury; nociceptive pain usually arise accompanying inflammation. Some mild chronic pain can be produced by sprains and strains, whereas the pain of arthritis or tumor invading soft tissues results in severe chronic pain. Neuropathic pain results from direct injury to nerves in the peripheral or central nervous system. Phantom limb is an example of neuropathic pain [18].

1.3.3 Nociceptors

Nociceptors are the sensory receptors that send neuronal signals to the spinal cord and the brain in response to the potentially damaging stimulus. Nociceptive neurons respond to extreme pain or temperature, and this process of nociception causes the perception of pain.

As compared to the peripheral axons, nociceptive neurons have a higher threshold and are relatively slowly conducting. According to the conduction velocity, the peripheral axons are divided into A, B and C fibers. A and B are myelinated fibers, whereas C fibers are unmyelinated. Furthermore, A fibers are divided into Aα, Aβ, Aγ and Aδ according to their conduction velocity. Aα has highest conduction velocity, and in a descending order, Aδ has a lowest conduction velocity. Aδ and C fibers are responsible for pain sensation [18, 19]. The conduction velocity of Aδ fibers in mammals is 5-30 m/s, whereas that for C fibers is only 0.5-2 m/s, which means for a pain signal to reach the brain it will take around one to three seconds[18, 19]. Aδ fibers carry pain signals caused by excess pressure as well as heat, and the pain is perceived as sharp and localized. The C fibers on the other hand cause a diffuse, burning sensation that tends to be persistent. C fibers are activated by various stimuli such as pressure, temperature, and chemicals that are released by the damaged cells in vicinity [18].

The immediate pain caused by the stimuli is carried by Aδ fibers; however, there is a pain sensation even after the withdrawal of painful stimuli, in which case the pain is carried by a C fiber. If the injured region is exposed again to stimulation, whether painful or with lesser intensity of pain, the perceived pain sensation is increased. This is due to a lower threshold of the receptors caused by the injury. This phenomenon is called hyperalgesia, which involves amplification of pain signals.

1.3.4 Conduction of Pain

The pathways for the conduction of pain are different from other somatosensory pathways. The primary pain neurons, nociceptors, form their first synapses on the dorsal horn of the spinal cord [18]. The cell bodies are located in dorsal horn of the spinal cord whose receptive endings are located in the periphery. The dorsal horn of the spinal cord makes synapses on neurons that project to the somatic sensory cortex via thalamus. As the axons move up in the spinal cord, they make synapses at the contra-lateral side of the nociceptive neurons, which then pass through the medulla. The axons are then projected to the thalamus where they make synapses on neurons that project to the somatic sensory cortex. Figure 1.6 shows the conduction of pain from periphery to central nervous system. There are five different ascending pathways to carry nociceptive information to the brain: spinothalamic, sinoreticular, spinomesencephalic, cervicothalamic and spinohypothalamic tracts[18].

The gate control theory (proposed by Ron Melzak and Patrick Wall, 1965) explains the pathways that descend from the brain to the dorsal horn at the spinal cord are capable of modulation of pain information in the spinal cord, and capable of preventing pain sensation to reach the brain.

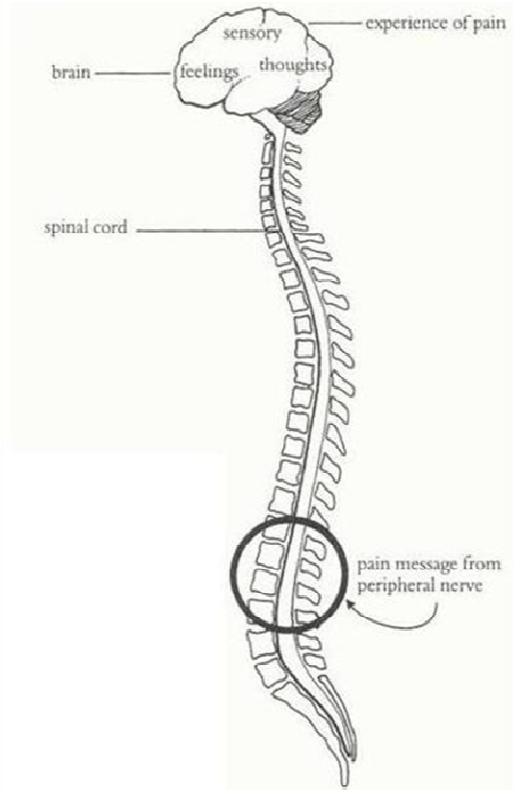

Figure 1.6 Pain pathway from periphery to Central Nervous system [43]

CHAPTER 2

PAIN STUDY

2.1 Aim of the study

The experience of pain is subjective in nature due to which the perception of pain in individual is very difficult to assess. Thus, the objective quantification of pain would help in evaluation and treatment of patients suffering from different pain-related diseases (such as chronic pain).

In recent decades, a number of functional neuroimaging methods have been used to study the pain processing in central nervous system[33]. Even though early clinical observations stated a minor role of the cerebral cortex in pain perception, various functional neuroimaging studies have reported the involvement of various cortical areas being involved in processing of pain[33,34]. Rather than a pain processing center, a network of cortical and sub-cortical regions constitute a pain matrix, which receive parallel inputs from multiple nociceptive pathways and are responsible for perception of pain. Prefrontal cortex (PFC), which is one of the cortical regions in the pain matrix, is responsible for the cognitive and attentional processing of pain. Also, the activities of medial PFC under the chronic pain condition were found to be altered with the intensity of chronic pain[35]. Thus, the ability to quantitatively assess pain perception using non-invasive measurement in the PFC would help patients who suffer from chronic pain and for patients who are in condition lacking communication (infants, coma). Thus the goal of my thesis study includes:

I. to assess brain activities in the PFC in response to the noxious pain stimulus;

II. to differentiate the hemodynamic activities in the PFC regions in response to two different levels of noxious pain stimuli;

III. to find neural correlates for cognitive evaluation of pain.

2.2 Materials and methods

2.2.1. Subjects

For this study, I recruited 7 healthy subjects from the University of Texas at Arlington (UTA) community. The age range of the subjects was 23 - 28 yrs old (Mean 25.1, S.D. 2.2). All of the recruited subjects were right-handed; prior to the study, the subjects did not have any neurological disorder and did not take any medication.

2.2.2. Instruments

2.2.2.1 CW6 Imager

CW6 (TECHEN Inc. MA) is an optical brain imager used in my study and is a multi-channel, continuous-wave (CW) system based on near-infrared spectroscopy (NIRS). The system consists of frequency-encoded lasers and an array of avalanche photo-diodes(APDs) detectors (see Fig. 2.1).

In our case, the system consists of 12 pairs of sources (24 in total); each pair consists two lasers at 690 nm and 830 nm. The power of the lasers can be adjusted as per the need, but typically it is set less than 10 mW. For my study, the 690-nm laser sources were set approximately around 6 mW, and 830-nm laser sources were set approximately around 3 mW. Each light source is modulated at a unique frequency ranging from 6.4 KHz to 12.6 KHz, with an increment of 200 Hz. Moreover, the system consists of 24 APD detectors. "Continuous parallel operation of all the sources and detectors allows for rapid data collection"[21].

CW6 system is an upgrade on existing CW5 system; CW6now consists of a real-time Digital Signal Processing (DSP) based control card. The real time DSP control card allows real time demodulation of signals. Thus, it makes the set-up more reliable, faster and easier as well as reducing the computing time for post-processing.

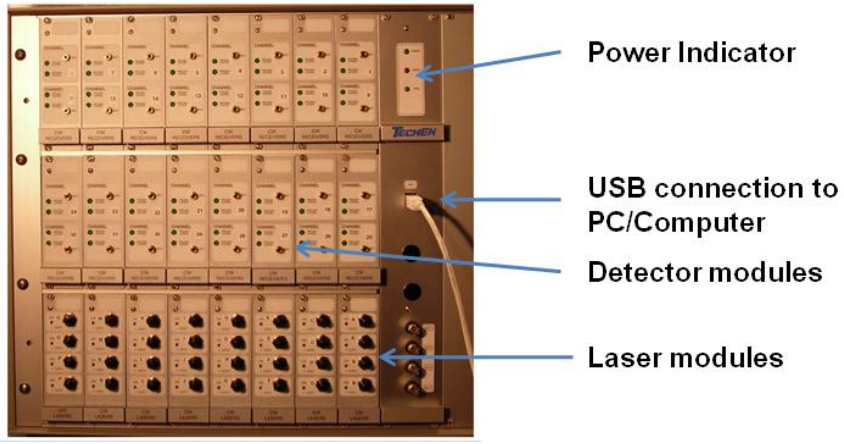

Figure 2.1 Front panel of CW6 Imager [21]

Each of the source module card consists of four lasers, and each pair with wavelengths of 690 nm and 830 nm are combined in pairs at the optode position (fig. 2.2 (a)). Similarly, the detector module card consists of two detectors (fig. 2.2 (b))

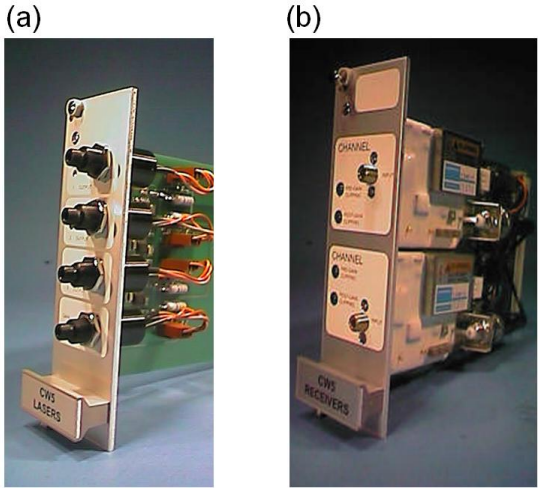

Figure 2.2 (a) Source module and (b) Detector module of CW6 [21]

2.2.2.2 Probe Geometry

The probe geometry configuration used for this study is as shown in fig. 2.3. A thermoplastic probe was used to fix the sources and detectors. A total of 8 sources (16 sources with 8 diode lasers from each wavelength) and 16 detectors were used in this study. All the sources were arranged in a middle row, which was equidistant from the top and bottom rows of the detectors (fig. 2.3). The distance between each row was 3 cm; the distance between a detector to detector sideways was 2.5 cm, and that between two rows of detectors vertically was 6 cm. Also, the distance between source to source was 2.5 cm. Thus, from this configuration we have a total of 28 source-detector pairs (channels) with source-detector separation being 3.2 cm. The total area covered by the CW-6 fiber probe was 25 X 6 cm^2.

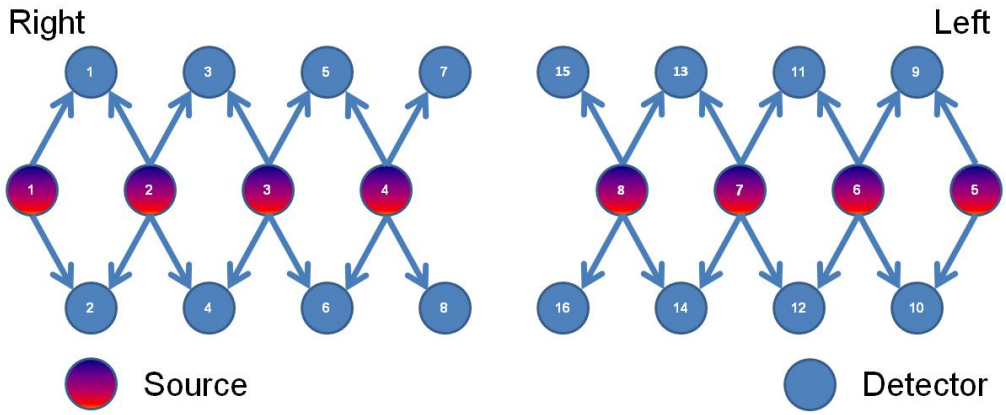

Figure 2.3 Source-Detector configuration

2.2.2.3 Pain Generator

Using a pneumatic device, a wide range of controllable innocuous as well as noxious pain can be generated[22]. A custom-built, pain generating pneumatic device [22] was used for this study. The pressure chamber has air pressure around 125-150 psi. The pressurized air is routed towards a voltage-to-pressure transducer (Marsh Bellofram Type 1000 transducer, 961-112-000). The transducer, which is an electro-pneumatic device, reduces the supply pressure(125 psi) to a regulated output pressure directly proportional to the electric input signal (0-10V). The two pressure gauges presented in fig. 2.4(a) monitor both the supply pressure and the regulated pressure. To set a required output pressure, an input voltage is set through a DC voltage controlled power supply. The voltage-to-pressure relationship curve is shown in fig. 2.4 (b). This regulated pressure will be used to propel the aluminum cylinder (12-mm diameter, 16.5-mm long, 4.69g in weight) from initial position **L** in the tube(144 mm long) to the final target position **T** when valve 1 is open (see fig. 2.4(a))**.** Ball valve is closed all the times to minimize the air pressure loss in the pressure accumulator. To retract the target back to the starting position **L o**f the cylinder, the ball valve must be open so that when valve 2 opens, vacuum pulls up the target back.

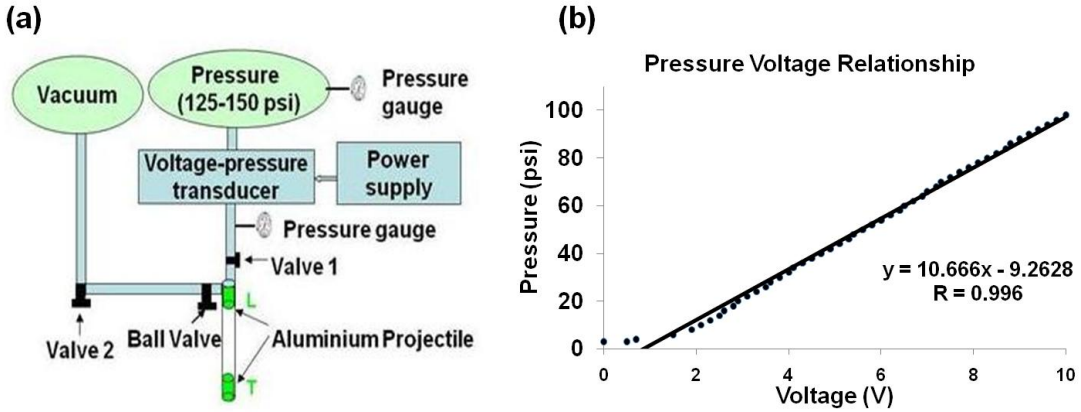

Figure 2.4 (a) Block diagram of a pain generator and (b) relationship between pressure and the control voltage of the voltage-pressure transducer.

2.2.3 Experimental Paradigm

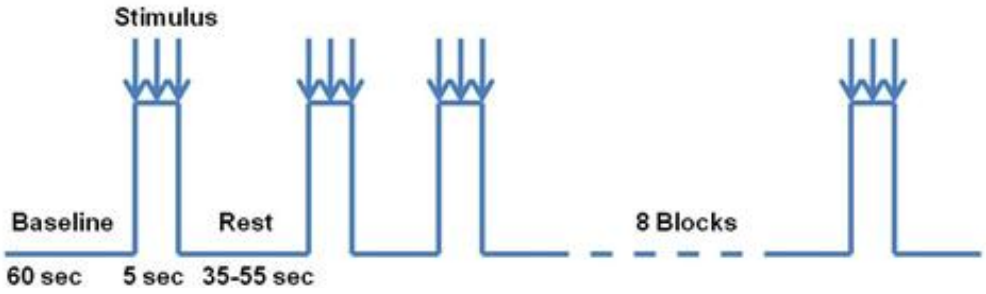

Figure 2.5 Experimental paradigm for the study

For my study, I followed a blocked-design protocol with variable inter stimulus interval (ISI). As shown in fig. 2.5, the measurement comprised an initial baseline of 60 seconds, followed by 5 seconds of a stimulus period. Within the stimulus period, the projectile was hit on the subject's volar forearm three times with 0.5 Hz. The design consists of 8 such stimulus blocks, and between those blocks the ISI was varied from 35 seconds to 55 seconds. The study was conducted across 2 visits, with a separation of 7-10 days between two visits.

2.2.4 Experimental set-up and procedure

A psychophysical study was conducted to estimate the magnitude of the pressure to be applied and its corresponding pain level generated on the subject. A stair-case approximation method was used where the pressure applied resulted in the lowest pain (0.3 V, 3 psi) and subjects were asked to rate the perception of pain using visual analog scale (0-10), as shown in fig. 2.6.

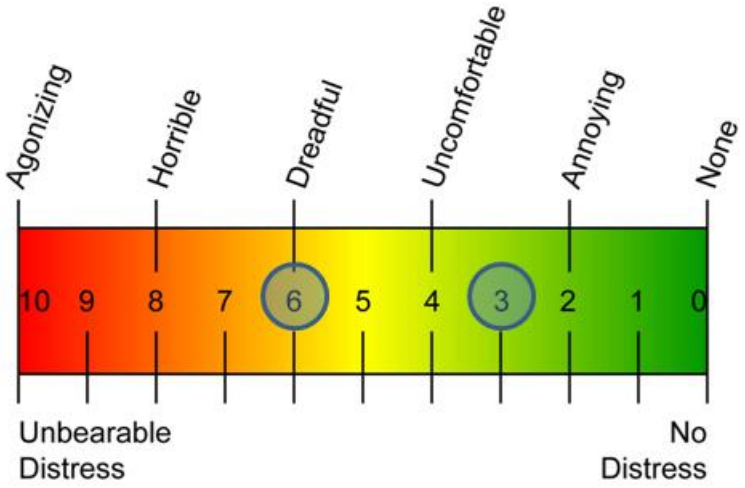

Figure 2.6 Visual Analog pain scale [58]

A total of 3 subjects participated for this psychophysical study. All the subjects were explained with pain rating procedures. Starting from a low power or voltage (0.3 V), the subjects was applied one stimulus each with an increase of 0.1 V power supply. After each stimulus, a 60-second ISI was applied, and the subjects were asked to rate their perception of pain verbally. The mean pressures corresponding to rating 3 (mean=1 V, Standard deviation=0.3 V) and 6 (mean=2 V, Standard deviation=0.2 V) were calculated. For my study, two levels of pain intensity were used, pain level 3 (1 V, 4 psi) and pain level 6 (2V, 10 psi) were used. For safety purpose, the pressure chamber was supplied with a pressure (27 psi) available in our laboratory.

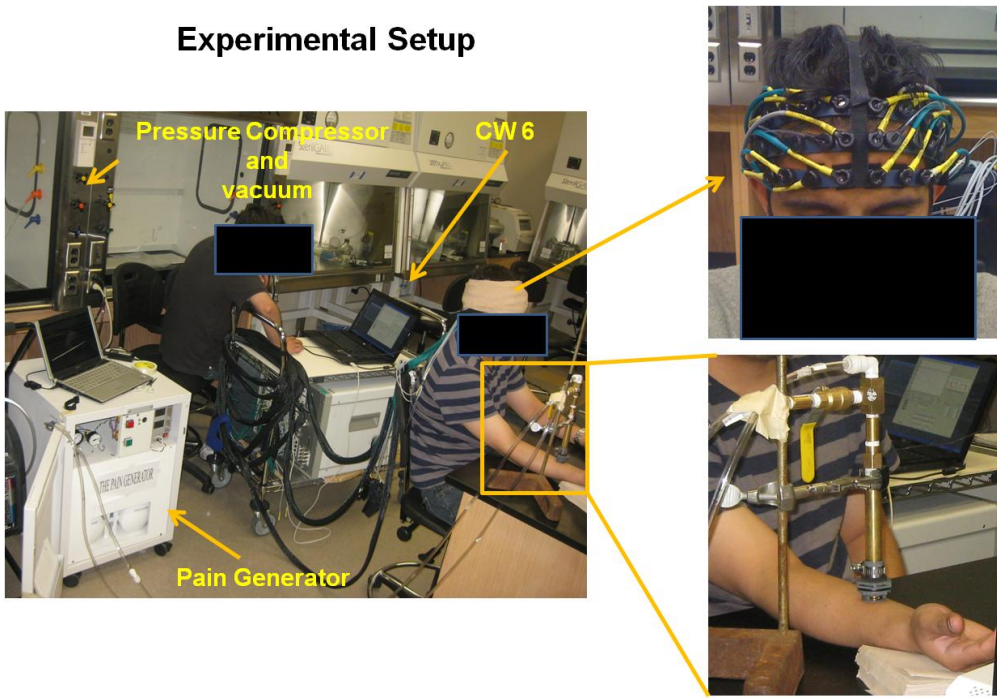

Figure 2.7 Experimental Set-up

The subjects were asked to comfortably seat in a chair. The head size was measured using a measurement tape, and nasion (Nz), Inion (In), and ears (AL, AR) were marked. All the marked area represents the 10-20 international system[23] of electrode placement. The probe was held tightly on the PFC area using velcro and elastic bandage strap to make sure the optodes are in contact with the scalp. Also, care was taken to remove the hairs in between optodes and scalp manually. To ensure the correct probe placement between two visits, the distance between Nz and the first row of the probe was measured. To block the ambient light, the probes were covered by an elastic bandage. The right hand of the subject (fig. 2.7) was rested comfortably on the table. The cylinder of pain generator was fixed on top of the right hand, where pain stimuli were applied. A stand was used to make sure that the cylinder would not put any weight on the forearm.

After the placement of probes and setup, the fNIRS signals were acquired over prefrontal cortex over the entire protocol period continuously. The subjects were explained about the experimental protocol, but they were not informed about the intensity of pain they would be getting. During the study, subjects were asked to close their eyes and concentrate on their right volar forearm where pain stimuli were applied. To make sure the timing of the stimuli were correct; a powerpoint presentation with timing information of the protocol was used. The study consisted of total of two visits; thus the subjects were asked to return in a span of 7-10 days. Using the recorded measurement of head distance, the probe was placed on the same position. After the end of the study each time, the subjects were asked to rate the average pain intensity using the visual analog pain scale (fig. 2.6).

2.2.5 Optode Co-registration

To find the neuro-anatomical position of the optodes, an international 10-20 system [23] of electrodes placement was used. Subjects were made to seat comfortably and the distance between nasion (Nz) to inion (In) and left ear (AL) to right ear (AR) were measured. Also, Cz is defined as central point between Nz-In and AL-AR was measured. Using a marker Nz, In, AL, AR and Cz position were marked. After the placement of probes on the subject's head, the co-ordinates of all the optodes along with Nz, In, AL, AR and Cz were recorded using a 3D Digitizer (Patriot Digitizer, Polhemus Inc). Then using NIRS-SPM, a freely downloadable Matlab-based software package from http://bisp/kaist.ac.kr/NIRS-SPM [24,25], the representation of spatial location of optodes on a human brain template were obtained.

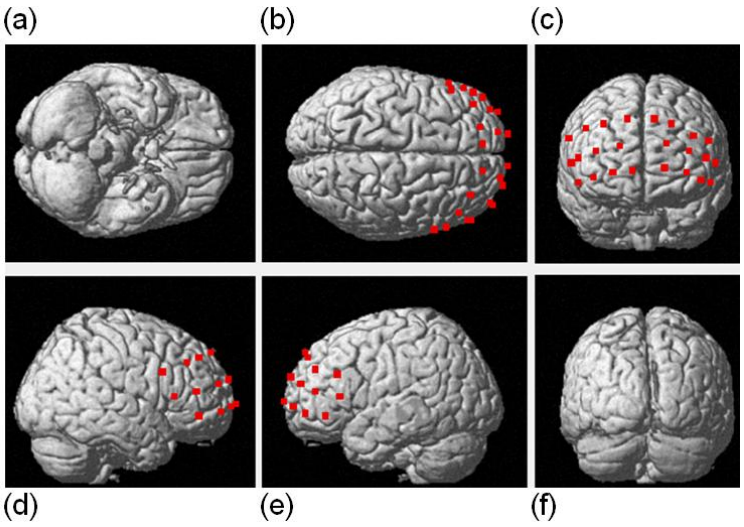

Figure 2.8 Optode co-registration on human brain template (a) Ventral view, (b) Dorsal view, (c) Frontal view, (d) Right Lateral View, (e) Left Lateral view, and (f) Occipital view

The positions of the optical optodes on the human brain templates are shown in figs. 2.8 (a)-(f). These figures provide the probe geometry overlaid on the cerebral cortex, showing that the areas covered by the optical probes correspond to Braodmann area (BA) 10 and some part of BA 9 and 46 [24, 25].

2.2.6 Behavioral Pain Rating

My study consists of two visits for measurements at two different pain levels. All the subjects were asked to rate the average pain intensity after the end of each measurement. For visit 1, low pain intensity of level 3 was used; for visit 2, moderate pain of level 6 as described in section 2.2.4 were used. Two group-averaged pain ratings for two visits are as shown in figure 2.9. The average pain rating for visit 1 was 3±0.3, and that for visit 2 was 6±0.4. The result here suggests that the perception of pain at higher pain intensity is significantly higher between two visits. A paired t-test analysis between two pain levels gives us a p-value of 0.0004, indicating a statistically significant difference in pain perception between low and moderate pain.

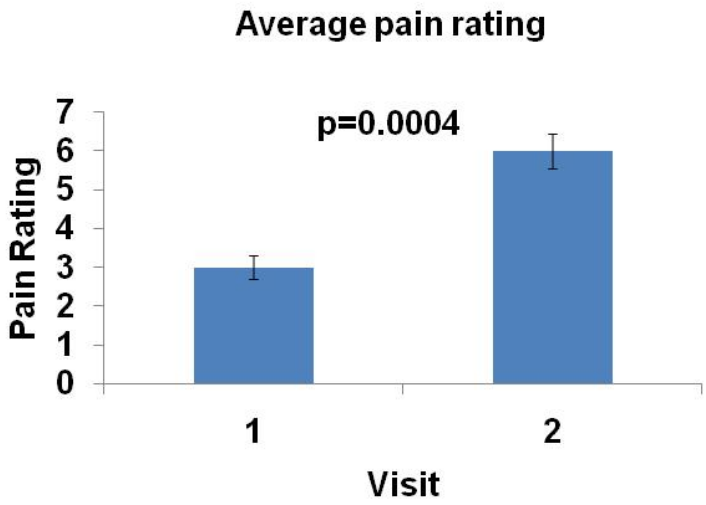

Figure 2.9 Group-averaged pain ratings over all the subjects (n=7) with two pain levels. Error bars here represent standard error of mean (SEM).

2.2.7 Data processing

The initial pre-processing of data was done using freely available Matlab-based software from http://www.nmr.mgh.harvard.edu/DOT/resources/homer/forum.htm. The software called HomER [26] is extensively used for the processing of fNIRS data.

General steps followed for the processing of data using HomER are shown in fig. 2.10: fNIRS data were checked individually for each channel; namely the raw optical intensities were assessed channel by channel. The channels showing large noise were further inspected by performing power spectral density (PSD) on the optical signals. Thus, the channels with significant noise and without characteristic frequencies (Heart beat and respiration) in their PSD were removed from further processing. The large noise may result from various factors, such as subject's high density or dark color of hair, imperfect probe placement on the scalp, and so on.

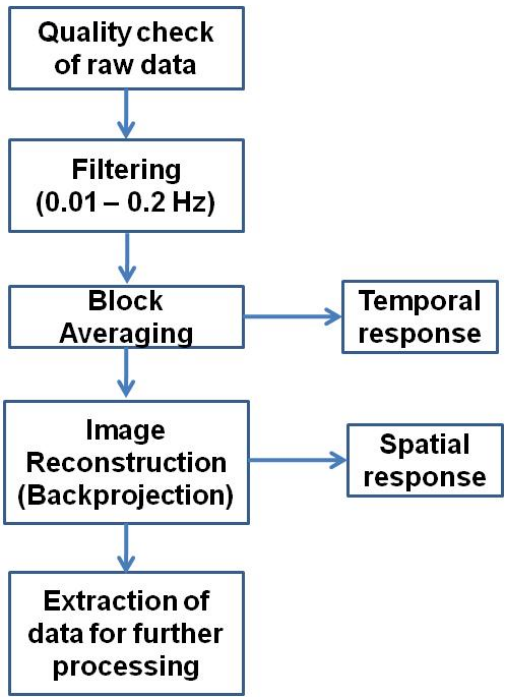

Figure 2.10 General steps followed in processing of fNIRS data

Apart from the signals coming from cerebral activation of the cortex, fNIRS signals consist of various other physiological components, such systemic physiological noise as cardiac pulsation, respiratory signal and systemic blood pressure. Also, due to the high sampling rate of the optical instrument, the fNIRS signals consist of instrumental noise as well [25]. Thus, to remove such noise in the signals as well as to correct the low-frequency baseline drift, the optical signals were band-pass filtered from 0.01 - 0.2 Hz. Then, using the stimulus timing information, the fNIRS signals were block averaged for 40 seconds (5 sec stimulation followed by 35 sec recovery);the temporal profiles of HbO and HbR were obtained [28]. Block averaging on all the channels will maximize the signal-to-noise ratio.

2.3 Experimental results

After initial pre-processing, the fNIRS data were extracted to Matlab for further processing. The HbO signals in fNIRS highly correlate with the BOLD signals in functional magnetic resonance imaging (fMRI) [29],which is currently considered as the gold standard in the field of functional neuroimaging. For this study, I focus on HbO signals.

For comparison of responses in PFC between resting state and during pain stimuli, I compared block-averaged temporal profiles of HbO in resting state as well as during both pain stimuli. The 5-minute baseline data taken before actual pain stimulation were block averaged using 40-sec as a block period.

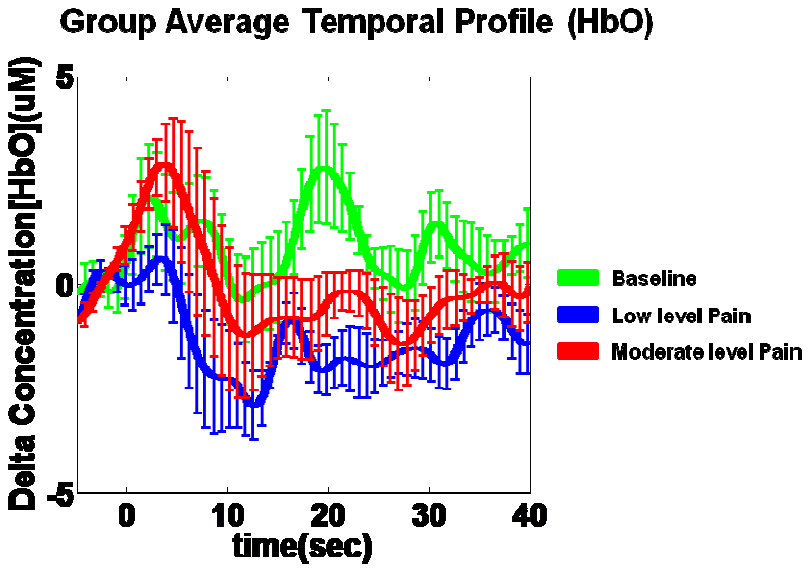

Figure 2.11 Group-average temporal profiles of HbO during rest and painful stimuli

Figure 2.11 shows three grand-averaged temporal profiles over all the channels in PFC across all seven subjects. For the comparison of temporal responses, a temporal correlation between the HbO signals taken during the baseline and pain stimuli for 0-20 sec was performed. The analysis between the baseline and low level of pain stimuli yielded a Pearson's correlation coefficient of 0.4 with a p-value of 0.03 (p-value here indicates the significant difference of correlation coefficient from zero). Similarly, analysis between the baseline and

moderate level of pain stimuli yielded a Pearson's correlation coefficient of 0.4 with a p-value of 0.03. However, temporal correlation between the low level of pain stimuli and moderate level of pain stimuli yielded Pearson's correlation of 0.8 with a p-value of 0.000001. This analysis here shows that the activity in PFC correlates highly under both pain stimuli. Thus, the results here imply that the PFC activities in response to pain stimuli are different from those during the baseline condition.

2.3.1 Cluster channels analysis

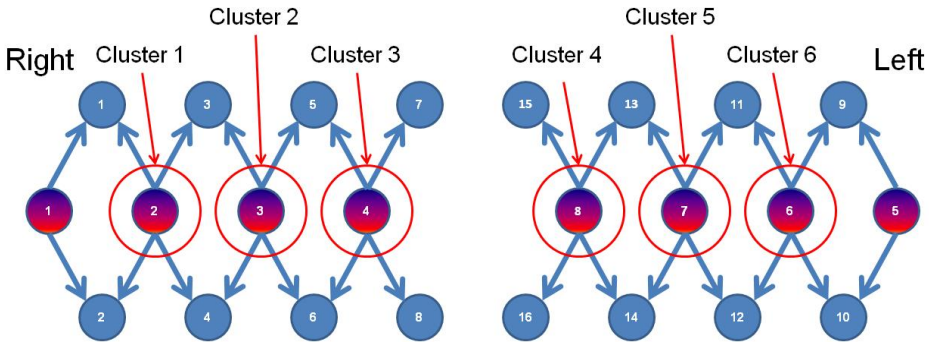

Figure 2.12 Division of clusters for cluster analysis

The HbO signals from all channels were block averaged. The temporal data were then exported for further data processing and analysis. Specifically, the channels were divided into six clusters (three clusters on each side of the PFC), as shown in fig. 2.12. Each cluster consisted of four channels, and the temporal profiles from each of the four channels were averaged. For group average analysis, all the four channels from seven subjects were grand averaged.

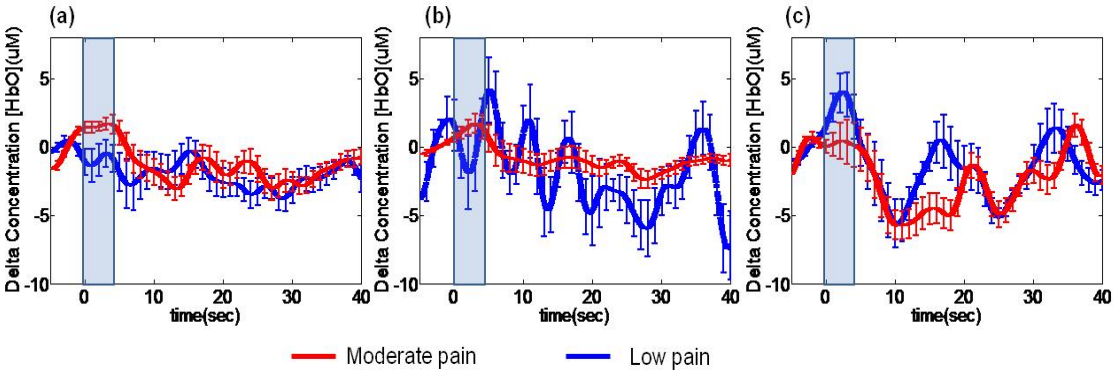

Figure 2.13 Grand average temporal profile (HbO) of ipsi-lateral side of PFC (a) Cluster 1, (b) Cluster 2 and (c) Cluster 3. Error bar represents SEM.

The grand averaged temporal profiles of HbO for all seven subjects are shown in fig. 2.13. The red and blue curves here represent temporal profile of HbO in response to the moderate level of pain and low level of pain, respectively. The temporal curves in fig. 2.13 represent the responses in the ipsi-lateral side (right side) of PFC. Figures 2.13 (a), (b) and (c) represent the temporal responses of HbO in cluster 1, 2, and 3, respectively (see fig. 2.12). The y-axis represents changes in concentration of HbO in micro-molar (uM), the x-axis represents time course in seconds. The shaded portions in fig. 2.13 represent the time period when pain stimuli were applied.

Similarly, fig. 2.14 shows the temporal profile of HbO in the contra-lateral side (left) of the PFC. The grand averaged temporal profiles of HbO for the contra-lateral clusters (fig. 2.14 a-c) are consistent between visit 1 and visit 2. Figures 2.14 (a - c) show a slight increase, followed by a decrease in HbO concentration. The visual inspection on temporal HbO profiles between visit 1 and visit 2 shows difference in response. However, the clusters in ipsi-lateral sides do not show such a pattern. It can be seen that HbO signals have stronger responses in the contra-lateral side of PFC than the ipsi-lateral side.

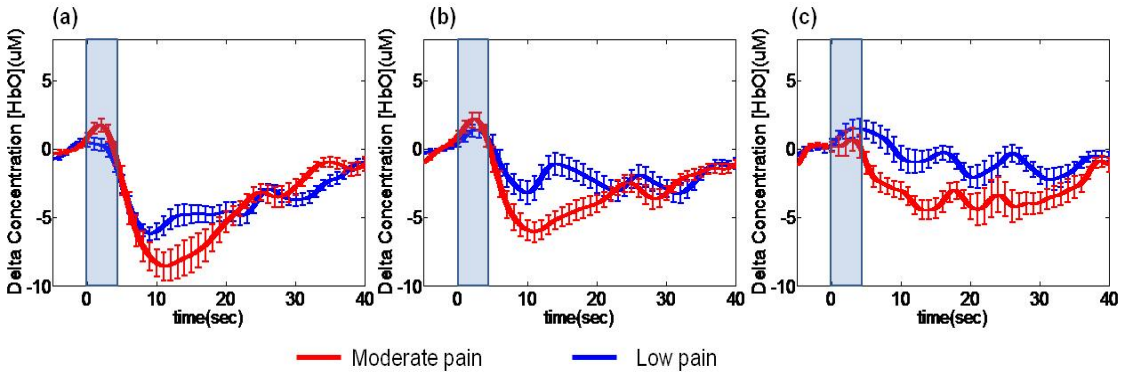

Figure 2.14 Grand averaged temporal profiles of HbO in the contralateral (left) side of PFC taken from (a) Cluster 4, (b) Cluster 5 and (c) Cluster 6. Error bars represent SEM.

2.3.2 Multi-parameter analysis

For further analyzing the HbO responses between two different pain stimuli, certain characteristic features were taken into considerations. To compare and contrast the brain response in PFC, parameters, such as maximum dip and time taken to reach such a dip, were selected as seen in fig. 2.15. These characteristic features were chosen because of their presence in all of the clusters.

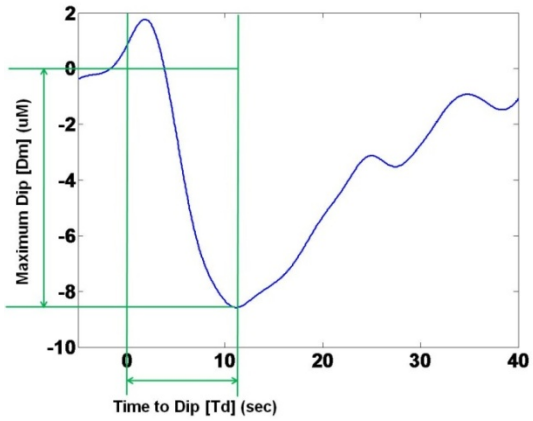

Figure 2.15 Parameters for temporal profile in cluster-based analysis

a. Maximum Dip (Dm) - Dm is the minimum of the HbO amplitude during the temporal response. It gives a single value of the HbO change in each curve. Figure 2.15 shows how

maximum dip (Dm) is defined in the temporal response. Comparison of Dm between two visits gives the estimate of difference in responses.

b. Time to Dip (Td) - Td is the time taken to reach Dm value in temporal response of HbO. It gives a single time to dip value in seconds. Figure 2.15 shows how time to dip (Td) is defined in the temporal profile. Comparison of Td between two visits gives the estimate of difference in responses.

2.3.2.1 Comparison of Maximum Dip

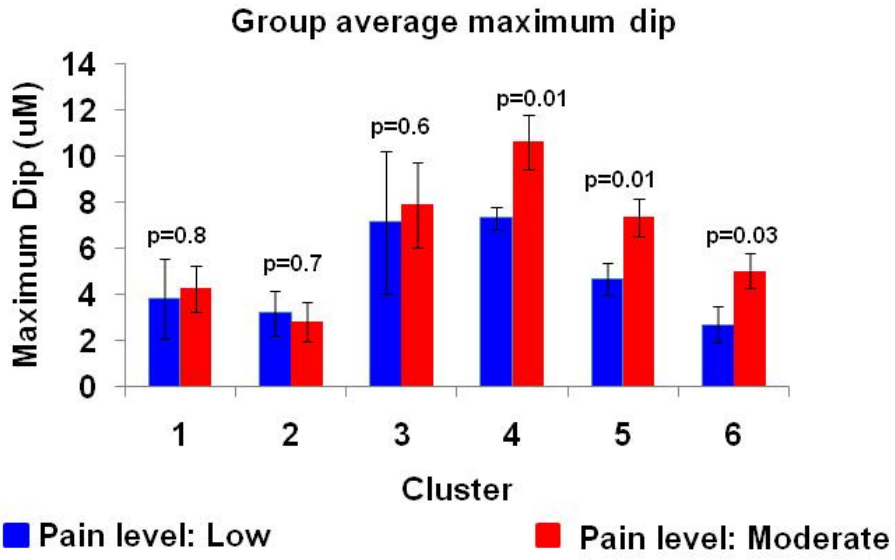

Figure 2.16 Group averaged comparison of Maximum Dip between two different levels of pain. Blue and Red bars represent maximum dip in response to low and moderate level of pain, respectively. Error bars represent SEM.

The maximum dip values of the temporal response for all the clusters were calculated. All the channels of each of the clusters over every subject were inspected individually. Then group averaged maximum dip for all the clusters were calculated by grand averaging the values. Similar steps were followed to calculate maximum dip for both levels of pain. Group averaged values of maximum dip for all the clusters are shown in figure 2.16. The group

averaged Dm values from cluster 1, 2, 3, 4, 5 and 6 in response to low level of pain stimuli were found to be -3.8±1.7, -3.2±1.0, -7.2±3.1, -7.3±0.5, -4.7±0.7 and -2.7±0.8, respectively. Similarly, the group averaged Dm values of cluster 1, 2, 3, 4, 5 and 6 in response to moderate level of pain stimuli were found to be -4.3±1.0, -2.9±0.8, -7.2±1.8, -10.6±1.2, -7.4±0.8 and -5.0±0.8, respectively. All the Dm values were in micromolar (uM). Also, for simplicity in visual inspection in fig. 2.16, the values were inverted into positive values.

From figure 2.16, it can be seen that apart from cluster 2, the average Dm values in response to moderate level of pain are higher than those with low level of pain. For statistical comparison of Dm between two different levels of pain intensity, a repeated measures mixed model ANOVA (analysis of variance) was performed (using SAS system software version 9.0). The p-values calculated from the analysis are also shown in figure 2.16. From the analysis, the p-values calculated were 0.8, 0.7 and 0.6 respectively, for clusters 1, 2, and 3, meaning that there is no significant difference in Dm between low and moderate level of pain stimulation in clusters 1, 2 and 3. However, the maximum dip values in response to moderate pain stimuli in clusters 4, 5 and 6 were significantly higher than those with lower level of pain stimuli based on the p-values of 0.01, 0.01 and 0.03, respectively. Thus, it can be concluded that the Dm values of all the clusters in the contra-lateral side were significantly higher in response to moderate level of pain as compared to those with low level of pain.

2.3.2.2 Comparison of Time to dip

The time-to-dip values of the temporal response from all the clusters were calculated. After the calculation of maximum dip, the corresponding times to reach Dm were calculated. The calculation was done for all the channels of each of the clusters of every subject individually. Then group averaged time-to-dip values for all the clusters were calculated by averaging all the values. Similar steps were followed to calculate time-to-dip values for both levels of pain.

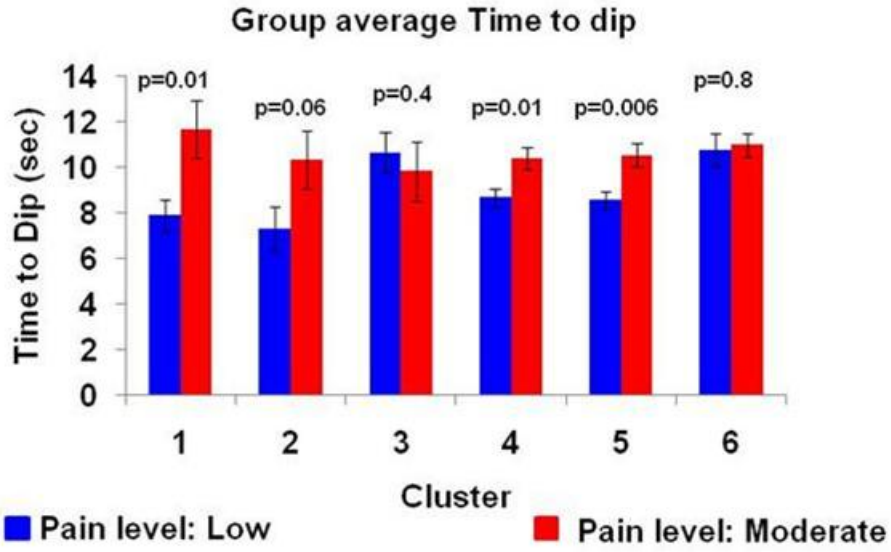

Figure 2.17 Group-averaged comparison of Time to dip between two different levels of pain. Blue and Red bars represent time to dip values in response to low and moderate level of pain, respectively. Error bars represent SEM.

The comparison of time to dip between two different levels of pain is shown in fig. 2.17. Error bars on the bar diagram represent standard error of mean. The group averaged values of Td in response to low level of pain stimuli for cluster 1, 2, 3, 4, 5 and 6 were found to be 7.9±0.7, 7.3±1.0, 10.7±0.9, 8.7±0.4, 8.6±0.4 and 10 .8±0.7, respectively. Similarly, the group averaged values of Td in response to moderate level of pain stimuli were found to be 11.7±1.3, 10.4±1.3, 9.9±1.3, 10.4±0.5, 10.6±0.5, and 11.0±0.5 . All the values were in seconds. Repeated measure mixed model ANOVA was applied for statistical analysis of the data. The p-values from the calculation are also shown in fig. 2.17. The p-values for cluster 1, 2, 3, 4, 5 and 6 are 0.01, 0.06, 0.4, 0.01, 0.006 and 0.8 respectively. Time to dip values for clusters 1, 4 and 5 were significantly higher in response to moderate pain stimuli than low pain stimuli.

Overall, clusters 4 and 5 show a significant difference in both maximum dip and time to dip between low and moderate levels of pain stimuli. Thus, it can be said that the contra-lateral region of PFC is able to show different responses to different levels of pain stimuli.

2.3.2.3 Behavioral versus Hemodynamic activity

To find possible correlation between characteristic features of the HbO temporal profiles (such as maximum dip and time to dip) and behavioral pain rating, a simple linear regression analysis was performed. After the calculation of average responses (i.e., Dm, Td) within each of the clusters, the regression analysis was performed. For simplification of calculation and visual inspection, Dm values were inverted in to positive magnitude. The R values calculated from the linear regression gives the correlation coefficient. Figures 2.18 (a) - (c) shows the linear regression between Dm and behavioral pain rating for cluster 1 - 3. The R values between Dm and behavioral pain rating for cluster 1, 2 and 3 were 0.05, 0.3 and 0.5, respectively, and their corresponding p-values were 0.9, 0.3 and 0.2. Similarly, the R-values for Td and behavioral pain rating for clusters 1, 2 and 3 were 0.13, 0.3 and 0.28, respectively, and their corresponding p-values were 0.7, 0.4 and 0.5(see fig. 2.18 (d) - (f)). The R values here suggest that the correlation between hemodynamic response (Dm, Td) and behavioral pain rating in response to low level of pain stimuli were low in ipsi-lateral clusters.

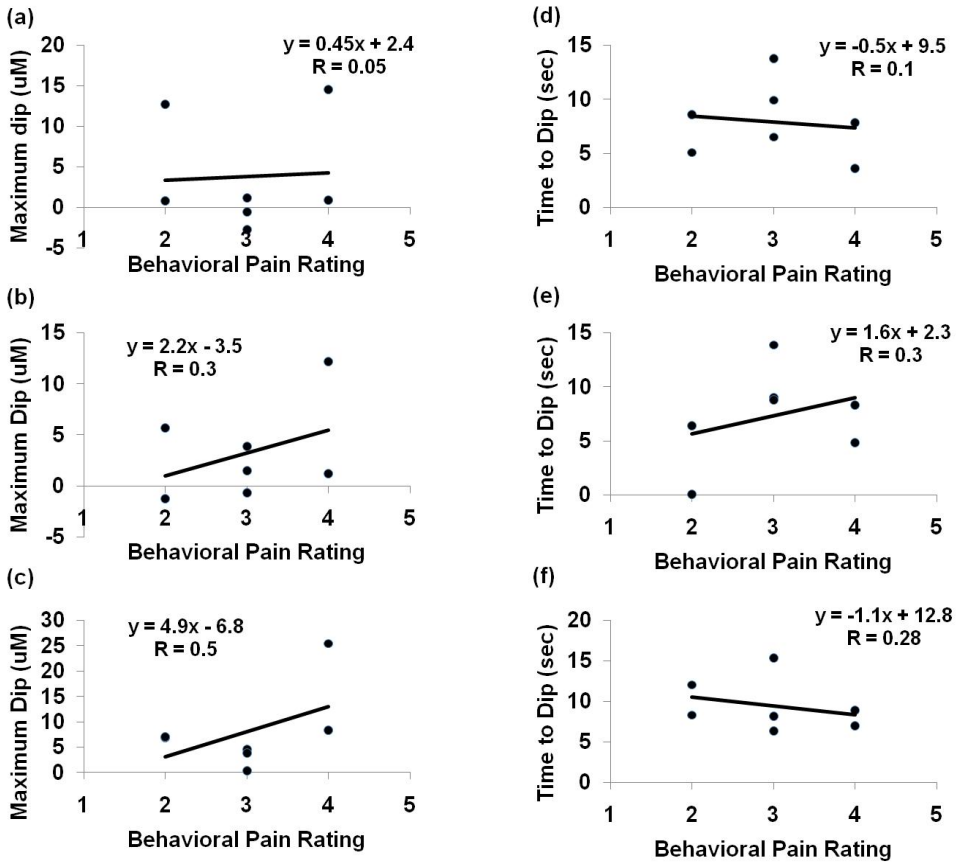

Figure 2.18 Linear regression analysis in response to low level of pain stimuli, (a)-(c) relationship between Dm and pain rating for cluster 1 – 3, respectively and (d) - (f) relationship between Td and pain rating for cluster 1 – 3, respectively.

The relationship between hemodynamic response (Dm and Td) with behavioral pain rating in response to low level of pain stimuli for cluster 4, 5 and 6 are shown in figure 2.19. Figure 2.19 (a - c), shows relationship of Dm, whereas fig 2.19 (d - f) shows relationship of Td. The R-values for Dm and behavioral pain rating for clusters 4, 5 and 6 were 0.04, 0.3 and 0.17, and their corresponding p-values were 0.9, 0.4 and 0.7, respectively. Similarly, the R-values for Td and behavioral pain rating for clusters 4, 5 and 6 were 0.6, 0.67 and 0.5, respectively, and their corresponding p-values were 0.1, 0.09 and 0.2. From R-values, Td values have better correlation (R>0.5) with behavioral pain rating than Dm.

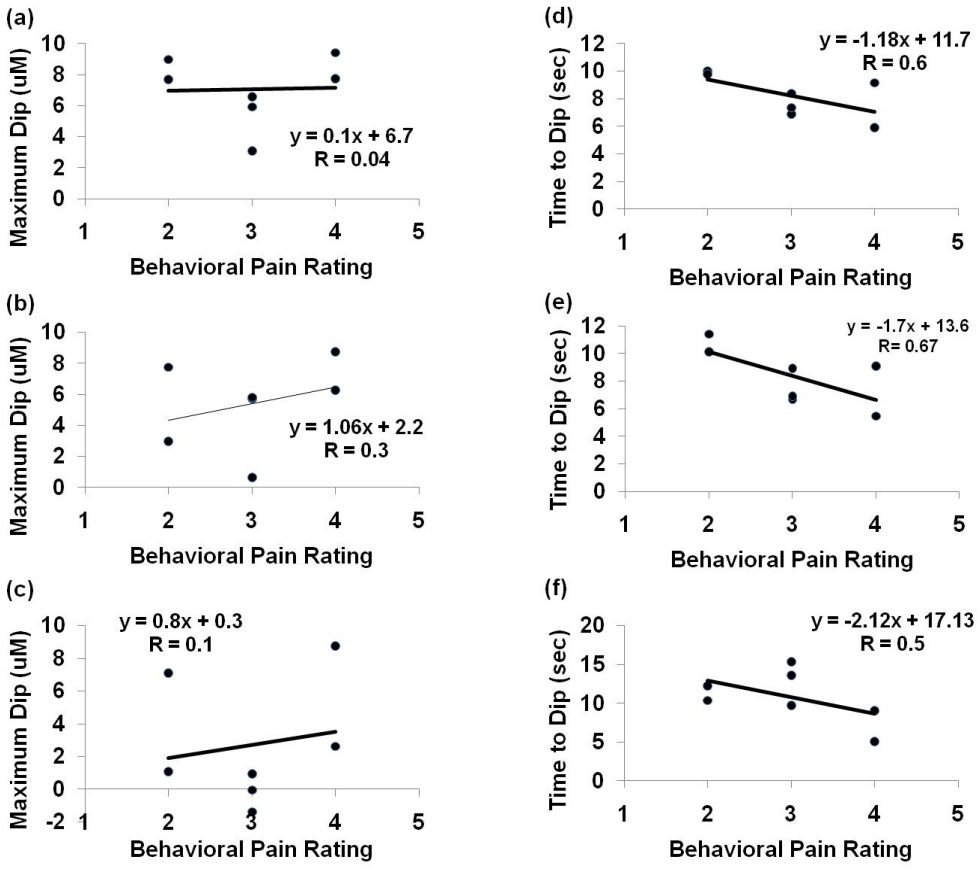

Figure 2.19 Linear regression analysis in response to low level of pain stimuli, (a) -(c): relationship of Dm with pain rating for cluster 4 – 6, respectively, and (d) - (f): relationship of Td with pain rating for cluster 4 – 6, respectively.

The relationship of hemodynamic response and behavioral rating in response moderate level of pain are shown in figures 2.20 and 2.21. Figure 2.20 (a - c) shows relationship between Dm and pain rating for cluster 1 - 3. Figure 2.20 (d - f) show the relationship between Td and pain rating for cluster 1 – 3, respectively. The R-values between Dm and pain rating for cluster 1, 2 and 3 in response to moderate level of pain stimuli were 0.48, 0.82 and 0.75, respectively, and their corresponding p-values were 0.2, 0.02 and 0.04.

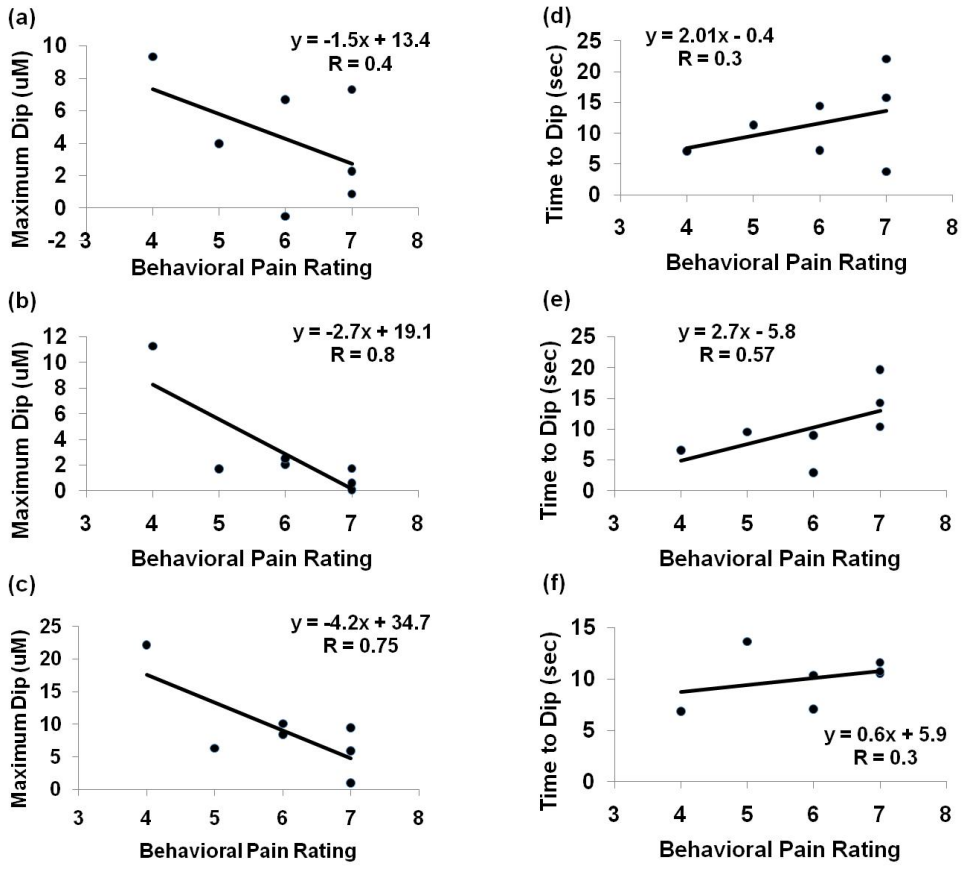

Figure 2.20 Linear regression in response to moderate level of pain stimuli. (a) -(c): relationship of Dm with pain rating for cluster 1 – 3, respectively, and (d) - (f) relationship of Td with pain rating for cluster 1 – 3, respectively.

Similarly, the R-values between Td and pain rating for cluster 1, 2 and 3 in response to moderate level of pain stimuli were 0.36, 0.58 and 0.3, respectively, and their corresponding p-values were 0.07, 0.04 and 0.5. From the R values, Dm and pain rating for cluster 2 and 3 have better correlation ($R \geq 0.7$).

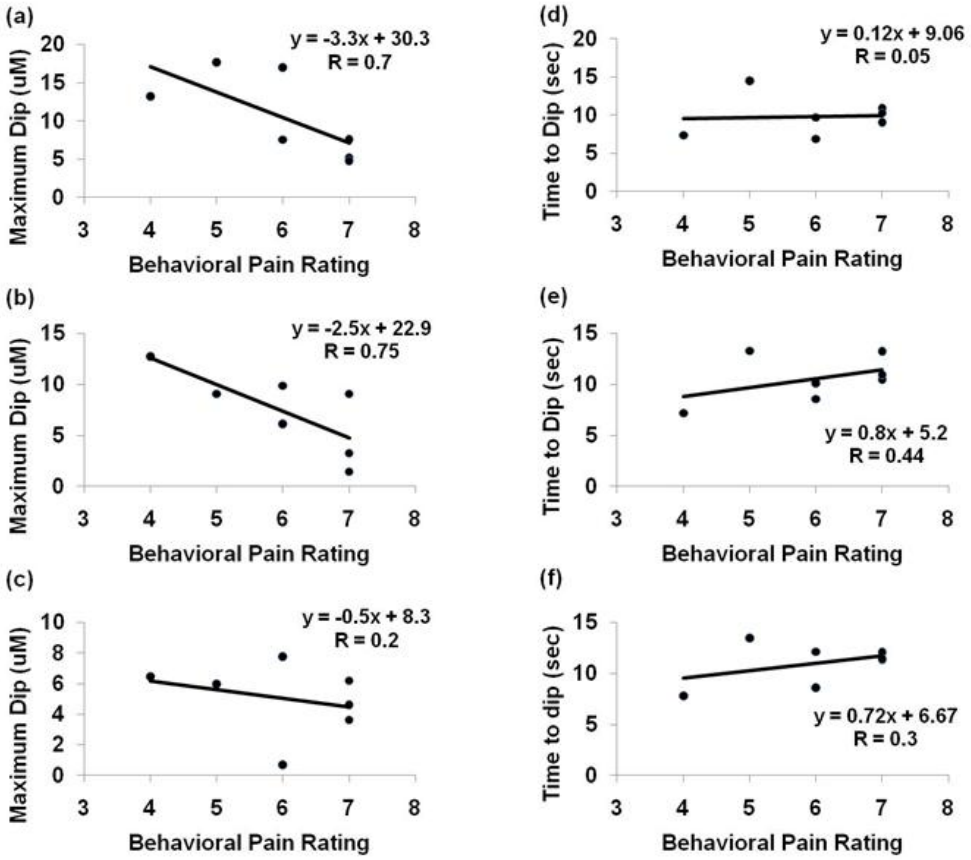

Figure 2.21 Linear regression in response to moderate level of pain stimuli, (a) -(c) relationship of Dm with pain rating for cluster 4 - 6 respectively and (d) - (f) relationship of Td with pain rating for cluster 4 - 6 respectively.

Figure 2.21 shows the relationship between hemodynamic response and behavioral pain rating for cluster 4 - 6 in response to the moderate level of pain. The R-values (fig 2.21(a - c)) between Dm and pain rating for clusters 4, 5, and 6 were 0.7, 0.75 and 0.27, respectively, and their corresponding p-values were 0.4, 0.1 and 0.4. Similarly, the R-values (fig 2.21(d - f)) between Td and pain rating for clusters 4, 5, and 6 were 0.05, 0.45 and 0.4, respectively, and their corresponding p-values were 0.3, 0.3 and 0.3. The correlation between Dm and pain rating for cluster 4 and 5 were higher ($R \geq 0.7$).

From figures 2.20 and 2.21, the correlations of Dm and pain rating for clusters 2, 3, 4, 5has R values greater or equal to 0.7. These four clusters (i.e., clusters 2, 3, 4 and 5) cover the medial prefrontal cortex (fig 2.8 and fig 2.10). Thus, it can be said that the maximum dip (in clusters 2, 3 , 4 and 5) and behavioral pain rating are highly correlated near the medial PFC in response to the moderate level of pain stimuli.

2.3.3 Region of interest analysis

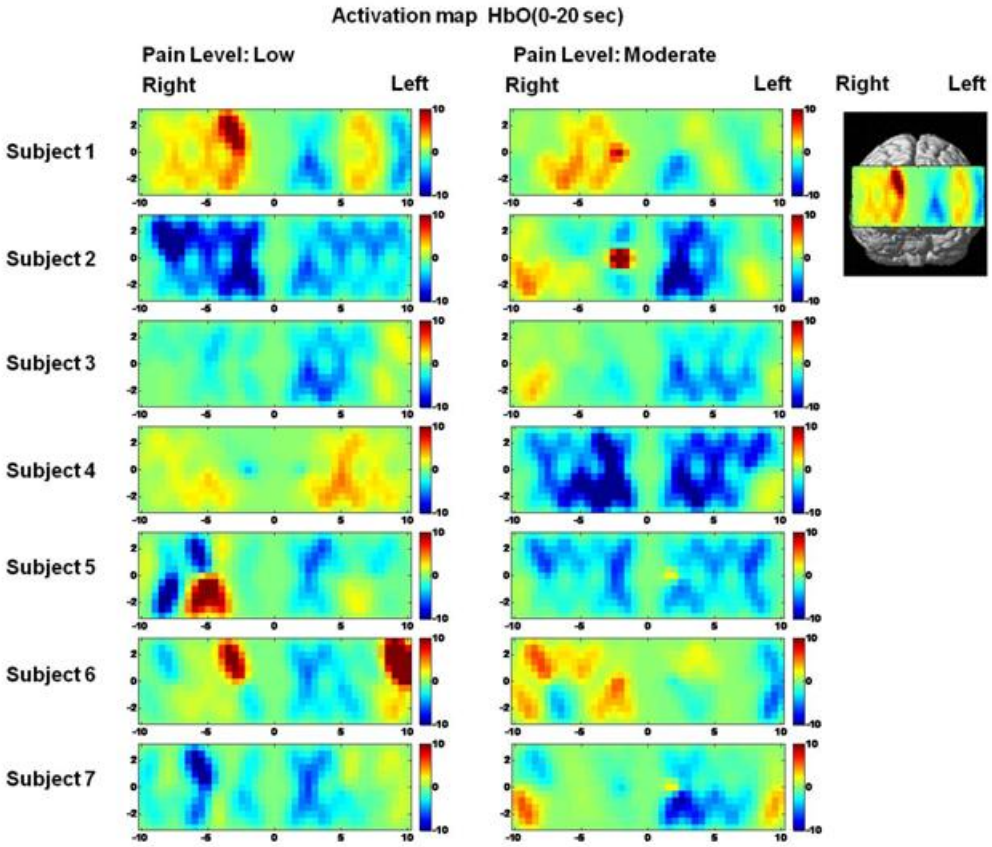

Figure 2.22 Activation map of HbO averaged temporally from 0 sec - 20 sec

The block averaging across each channel gives the temporal profile of HbO, HbT and HbR. Using the regular back-projection method in HomER software [26], we can reconstruct a two-dimensional (2D) spatial activation map of averaged functional activation across a selected temporal window. The activation image is reconstructed by generating a light-sensitive matrix based on probe geometry and a semi-infinite diffusion model[28]. Thus, solving the inverse matrix, absorption changes across the spatial distribution are calculated. Thus, the HbO, HbR and HbT concentration changes can be calculated using modified Beer-Lambert's law [7, 28, 30]. The spatial resolution (pixel size) chosen was 0.5 cm x 0.5 cm.

The activation map of HbO shows the spatial distribution of HbO changes induced by pain stimuli. From the cluster-based analysis (section 2.3.1), it can be seen that it takes approximately 20 second to reach the maximum dip and recover towards baseline. Thus, we define two time periods :(1) 0-20 seconds as the response period to pain stimuli and (2) 20-40 seconds as the recovery period. Figure 2.22 shows the spatial activation map averaged from 0 seconds to 20 seconds. The left and right columns of activation images represent the spatial activation map of HbO in response to low level of pain and moderate level of pain, respectively. There is an insert on top right corner of fig. 2.22, which is an activation map overlaid on top of a brain template for a representation of spatial distribution of HbO on PFC. Similarly, figure 2.23 represents the spatial distribution of HbO changes averaged from 20 to 40 second. From these activation maps, left aPFC areas show consistent deactivation, and also the activation appears less during the recovery period than that during the response period.

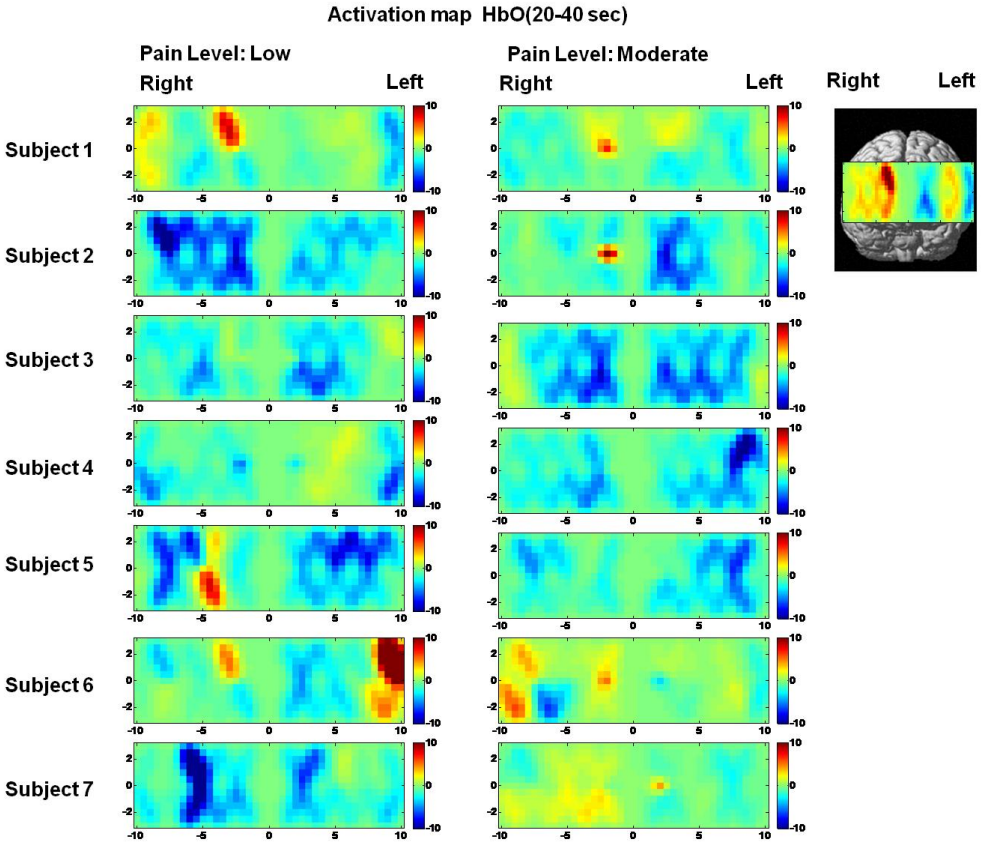

Figure 2.23 Activation map of HbO averaged temporally from 20 sec - 40 sec

The group level one-sample paired t-test was performed. A pixel-wise one-sample paired t-test would determine the regions that are significantly activated or deactivated from the baseline. For the calculation of group level t-map, pixel-wise changes of HbO for all the subjects were taken into considerations. Figures 2.24 (a) and 2.24 (b) show the region with significant deactivation in response to the low and moderate level of pain stimuli, respectively. Brown regions shown in the maps represent the regions with p values less than 0.01.

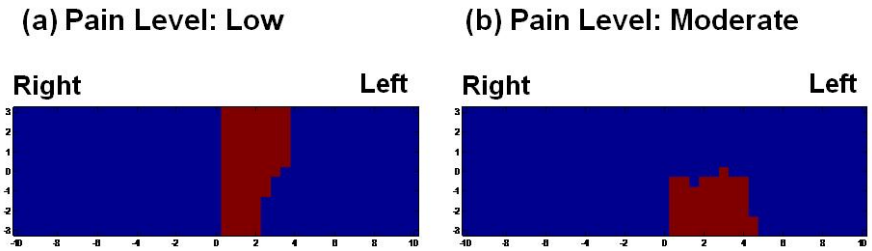

Figure 2.24 Group level t-test with (a) a low level of pain stimuli and (b) a moderate level of pain stimuli. Brown region in each map shows the region with significant response ($p<0.01$)

The pixels on the bottom left of the PFC region were common to both of the pain levels and thus selected as region of interest (ROI) for further data analysis. The ROI chosen is re-plotted in figure 2.25

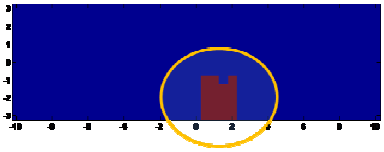

Figure 2.25 Region of Interest

Figure 2.26 shows the temporal profiles of averaged HbO values in response to low and moderate level of pain stimuli within the ROI. The error bars in the graph represent the standard error of mean.

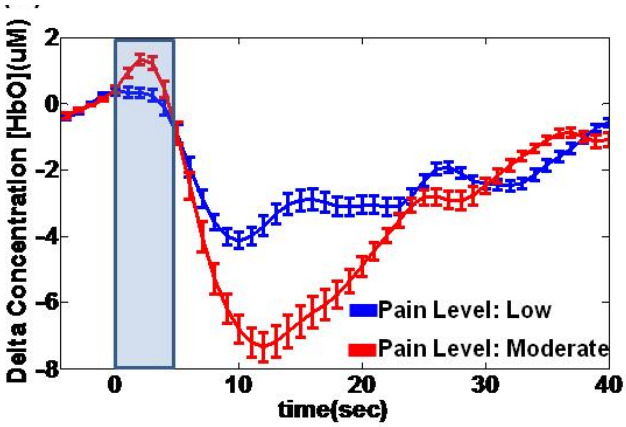

Figure 2.26 Averaged temporal profiles of HbO obtained within the Region of interest. Blue and red curves show the temporal profiles in response to low level and moderate level of pain, respectively. Error bar represents SEM.

The temporal profiles of HbO from region of interest are shown in figure 2.26. For the comparison of responses between different pain stimuli, the parameters discussed in section 2.3.1 (fig 2.15) were taken into considerations. Figures 2.27 (a) 2.27 (b) show the values of Dm and Td in response to different levels of pain stimuli; the temporal profiles of each pixel within the ROI were taken into consideration. For the statistical comparison, a repeated measures mixed model ANOVA was applied to the data. The p-values are shown on the top of the bar. The p-value for Dm and Td in response to low level of pain and moderate level of pain in ROI were 0.0005 and 0.1 respectively.

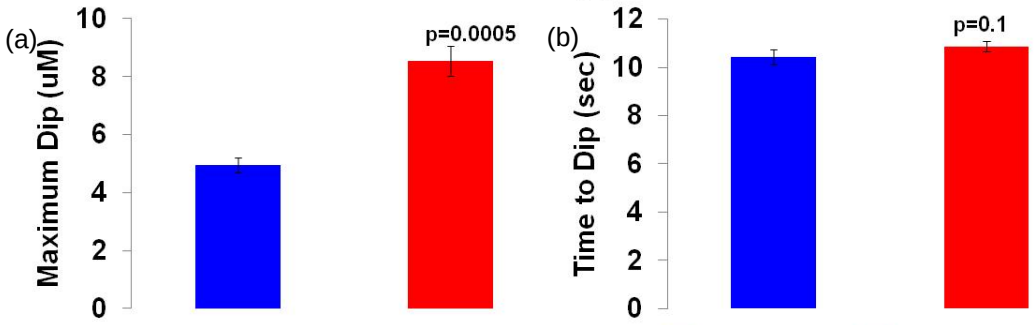

Figure 2.27 (a) Averaged Maximum Dip and (b) Averaged Time to Dip within the Region of interest. Error bars in the bar diagram represent SEM.

In summary, a significant difference in Dm is observed from the contra-lateral PFC in response to different levels of mechanical pain stimuli. The conclusion in this study is similar to some of the previous studies[44-46].

In this study, we see strong deactivation of HbO signals as opposed to the activation seen in many other studies. However, our results are in agreement with one of the pain studies using fMRI[47], which shows similar deactivation in medial PFC(see fig 2.28). Deactivation of HbO response suggests decrease in concentration of oxy-hemoglobin in that area. Even though there is no clear explanation about such deactivation we observe, some literature has provided certain explanation or expectation [48-50]. The deactivation of HbO might be due to a decrease in neuronal activity in prefrontal cortex. However, the physiological reason of deactivation is not well understood. Some of the studies have suggested that the deactivation was due to the poorly understood mechanism of vascular regulation, which suggests an increase in blood flow in certain regions from nearby regions. Also, as reported in many of the studies, PFC is associated with the spontaneous brain activity[51]. One of the reasons for deactivation in prefrontal cortex has been linked to the suspension of spontaneous brain activity due to the task[49].

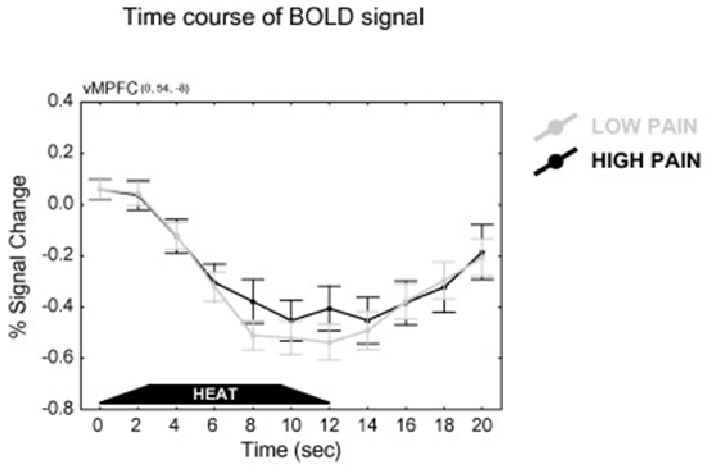

Figure 2.28 Time course of BOLD signal in response to Pain stimuli in PFC[47].

CHAPTER 3

PSYCHOLOGICAL STUDY

3.1 Aim of the Study

Stroop test[32] is a commonly used psychological test for attention and cognitive control of human brain. Cognition as we know is termed as the "process of thought". Thus cognitive psychology is a division of psychology which studies how people perceive, remember, think and solve problems[36]. In Stroop test, a name of color is displayed in different color than what the name means itself. It is easier to read the word itself, however, in order to name color of the word one has to manage his attention by inhibiting or interfering one response and promoting another response. Thus, Stroop test can be used to assess the cognitive operations of human brain structures[37].

The anterior prefrontal cortex (aPFC), Broadmann area (BA) 10 covers a large portion of frontal region of human brain. The fact that BA 10 is larger in human than in other primates and its development in latter stage of life suggests it is responsible for cognitive functions. Some of the functional neuroimaging have reported activity in BA 10 while performing working memory, problem solving, and decision making task[12-14]. However "the role of aPFC in cognition is least well understood" [11] Thus the goal of our study was:

I. to assess activity in aPFC during a psychological test
II. to differentiate the role of aPFC in Stroop inhibition
III. to find a neural correlate for cognitive function in aPFC

3.2 Materials and methods

3.2.1 Subjects

A total of 7 healthy male subjects (Mean Age 23, Standard deviation 3) from UTA community participated in the study. All of the subjects participating in the study had no prior neurological disorder and did not have any vision defect.

3.2.2 Instruments

3.2.2.1 Cephalogics high density diffuse optical tomography Imager

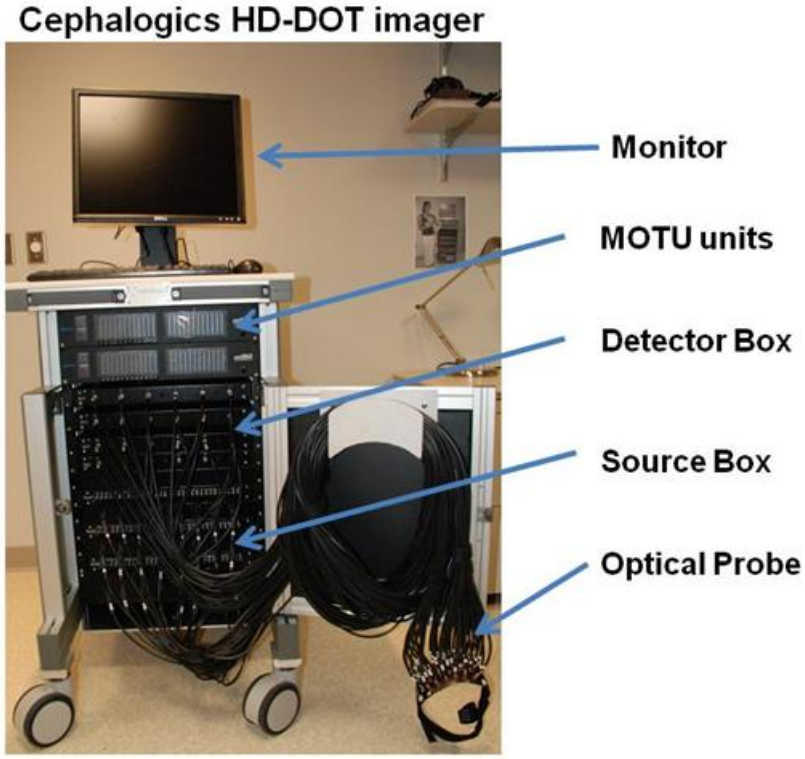

Figure 3.1 Cephalogics HD-DOT brain imager[57]

Cephalogics (Cephalogics LLC,MA) High Density diffuse optical tomography (HD-DOT) is a continuous wave optical imager used in functional brain imaging. The instrument has sources with two wavelengths, 750 nm and 850 nm. Each of the source consists of three 750 nm LEDs and one 850 nm LED. The power of 750 nm LED and 850 nm LED are set to 1.2 mW and 1.6 mW respectively. The sources with two different wavelengths are modulated at different frequencies. The detectors used are Hamamatsu APDs. The source and detector box are shown in figure 3.1. Also, the system has a MOTU unit which consists of 24 bit analog-to-digital converters (ADCs). All the detector channels are digitized with dedicated 24-bit ADCs and the sources are encoded (frequency-, time-, spatial-encoded). The ADC has a sampling frequency of 96 KHz which provides high instantaneous dynamic range and better cross-talk rejection[31].

3.2.2.2 Probe Geometry

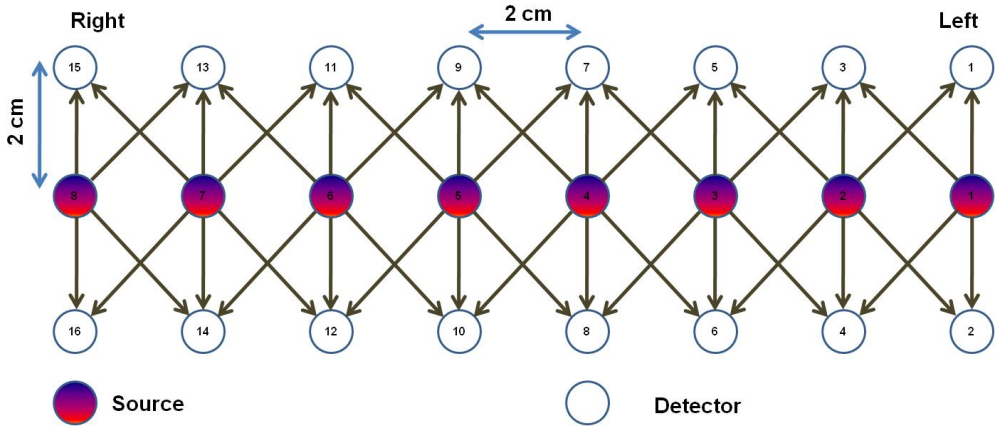

Figure 3.2 Probe Geometry

The probe geometry configuration used for the study is as shown in the figure 3.2. The total number of source and detectors used are eight and sixteen respectively. The source detectors are configured in the three rows as shown in the figure with source rows in the middle. The distance between source to detector and detector to detector was 2 cm. The first nearest source-detector separation was 2 cm and the second nearest source-detector separation as 2.8

cm, which makes the total number of channels as 44. The total area covered by the probes was 4 X 14 cm^2.

3.2.3 Experimental paradigm

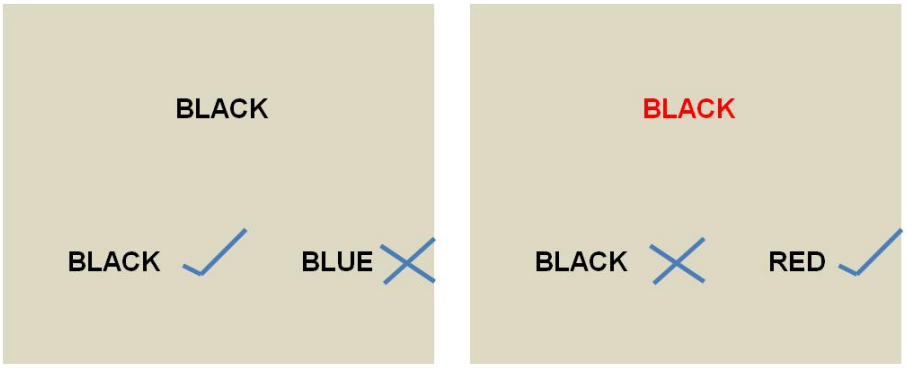

Figure 3.3 Example of two sessions used for study

For our study, matlab based computerized and modified Stroop test was used. The protocols used in the study consist of two sessions. The first session, namely word matching task (WM), is a simple task where a word (in black color) is displayed in screen and you have to match the word using a mouse. The second session, namely color word color matching task (CWCM), is a task where the name of a word is written in different color. One has to match the color of the word rather than the name of the word. For this we have used seven different colors (BLACK, WHITE, RED, GREEN, BLUE, CYAN AND MAGENTA) as stimuli. Figure 3.3 shows an example of both sessions. In session 1 (WN) task, you just have to match the name of the color. But in session 2 (CWCM task), the color name BLACK is written in RED color, thus you have to select option RED instead of option BLACK.

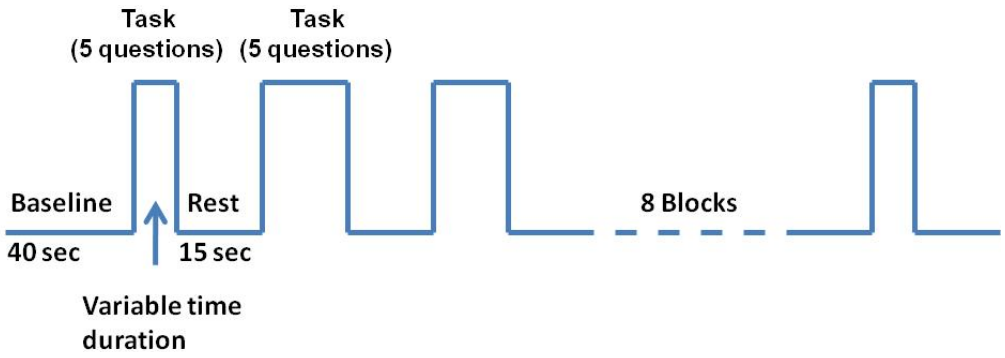

Figure 3.4 Block diagram of experimental paradigm

Before the data acquisition, a practice session was provided to each subject in order to be familiar with the protocols. The experimental paradigm consists of an initial baseline of 40 seconds, followed by eight blocks of task-rest sequence. Within a task block, five blocks of questions were given to subjects. The subjects were asked to answer the questions as fast and as accurate as possible, but there was no time constraint. Followed by a task is a resting period of 15 seconds as ISI. The experimental paradigm is shown in figure 3.4.The protocol used mouse pointer to select the correct answer rather than using '→' and '←' in conventional protocol which may result in a longer reaction time.

3.2.4 Experimental set-up and procedures

Using a measurement tape head size were measured (see section 2.2.4) [23]. The subjects were explained about the protocols and were provided with a practice session to make them familiarize with our protocol. The probe setup and experimental setup are shown in figure 3.5(a) and (b).After the probe placement and setup, fNIRS signals were acquired on aPFC over the entire protocol. The subjects were asked to seat comfortably and concentrate on the center of screen. In between two sessions, a short break of five to ten minutes was taken.

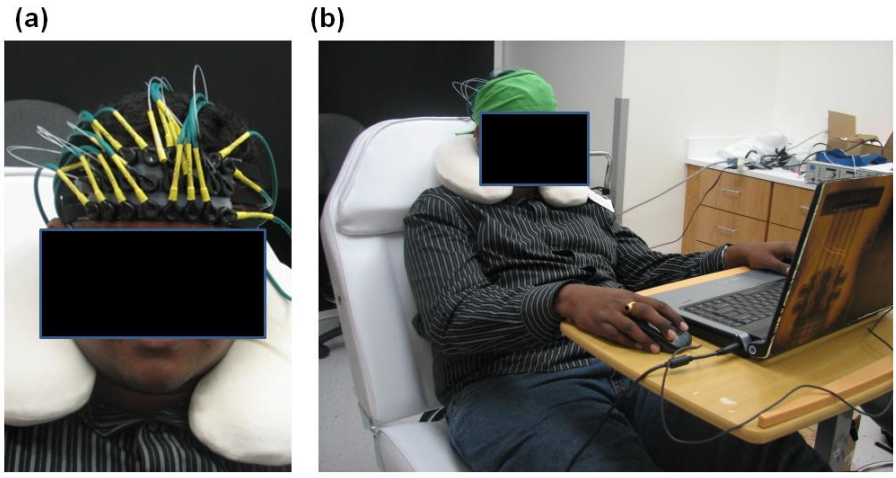

Figure 3.5 Experimental set-up

3.2.5 Optode Co-registration

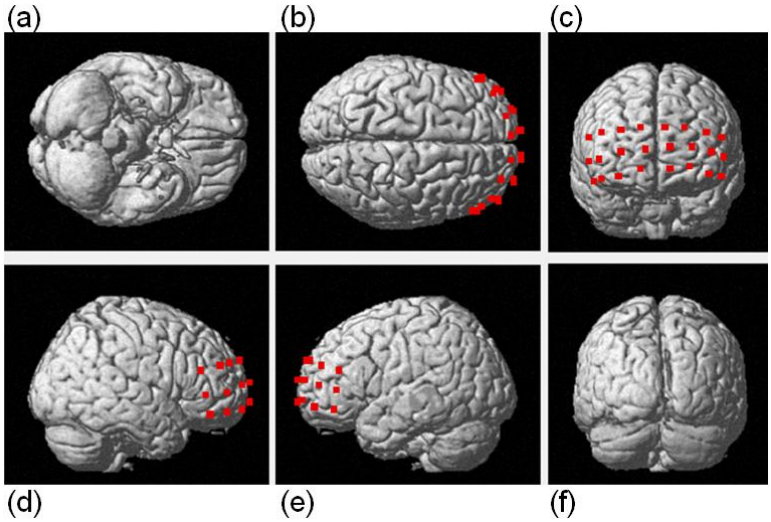

Figure 3.6 Optode co-registration on template (a) Ventral view, (b) Dorsal view, (c) Frontal view, (d) Right Lateral View, (e) Left Lateral view and (f) Occipital view

The process is discussed in details in section 2.2.5. Using 3 D digitizer, the position of the optodes in the human brain templates are shown in fig 3.6 (a-f). The majority area covered by the probe was BA 10. [24,25]

3.2.6 Behavioral Results

The reaction time to complete the task for each block was recorded. The reaction time represents the time taken by an individual subjects to complete five questions within a block. The recording data were taken for all the seven subjects during both sessions. The group average reaction times were 8.52±1.05 sec and 11.35±0.78 sec to complete a block for WM and CWCM task respectively. Since we are considering reaction time as a time to complete a single block with five questions, the reaction time was higher than that in conventional Stroop test. Figure 3.7 shows the group average reaction time of all subjects to complete WM and CWCM task. For the statistical comparison, a repeated measures mixed model ANOVA was performed on the data. The p-value calculated between reaction time of two sessions was 0.007. Thus, the reaction times between two sessions were significantly different.

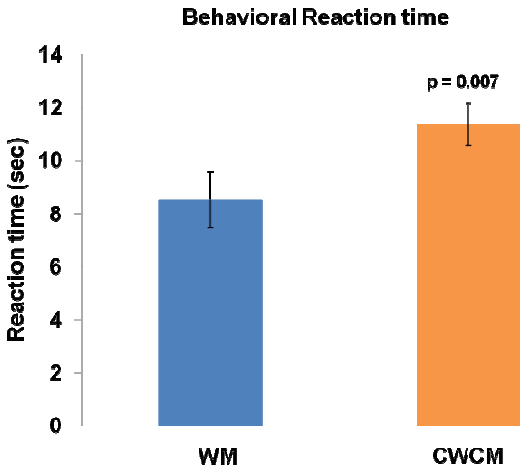

Figure 3.7 Group average behavioral reaction time during task. Error bar represents SEM.

3.2.7 Data processing

The details of data processing are discussed above in section 2.2.7 (fig 2.10). To filter out the physiological noise and instrumental noise [25] as well as to correct the baseline drift, a band pass filter of 0.01 Hz to 0.2 Hz applied to the fNIRS optical data. Also, from the reaction time, the shortest reaction time during a complete session was taken and the fNIRS signals were block averaged adding 15 seconds of rest period. Thus, the block averaged temporal profile of HbO, HbR and HbT are obtained for further processing of data[28].

3.3 Experimental Results

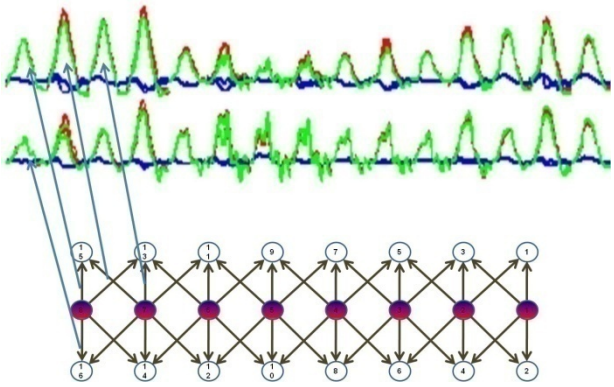

Figure 3.8 Representation of channels in temporal profile

The representations of the channels in the temporal profile are as shown in fig 3.8. The block averaged temporal profile of HbO, HbR and HbT across all the channels are shown in figure 3.9. The left column represents the temporal profile while performing WM task for all seven subjects. Similarly, the right column represents the temporal profile while performing CWCM task for all seven subjects. The green, blue and red curve represents the block averaged temporal profile HbO, HbR and HbT respectively.

Here, we can see the activation pattern of HbO is consistent throughout all the channels. Also, for all the subjects the temporal profile of HbO is similar during both WM and CWCM. However, the there is no such distinct profile found in HbR. Also as discussed in the above section, the HbO signal correlate highly with the BOLD signal in fMRI as well, thus we consider HbO signal for further analysis.

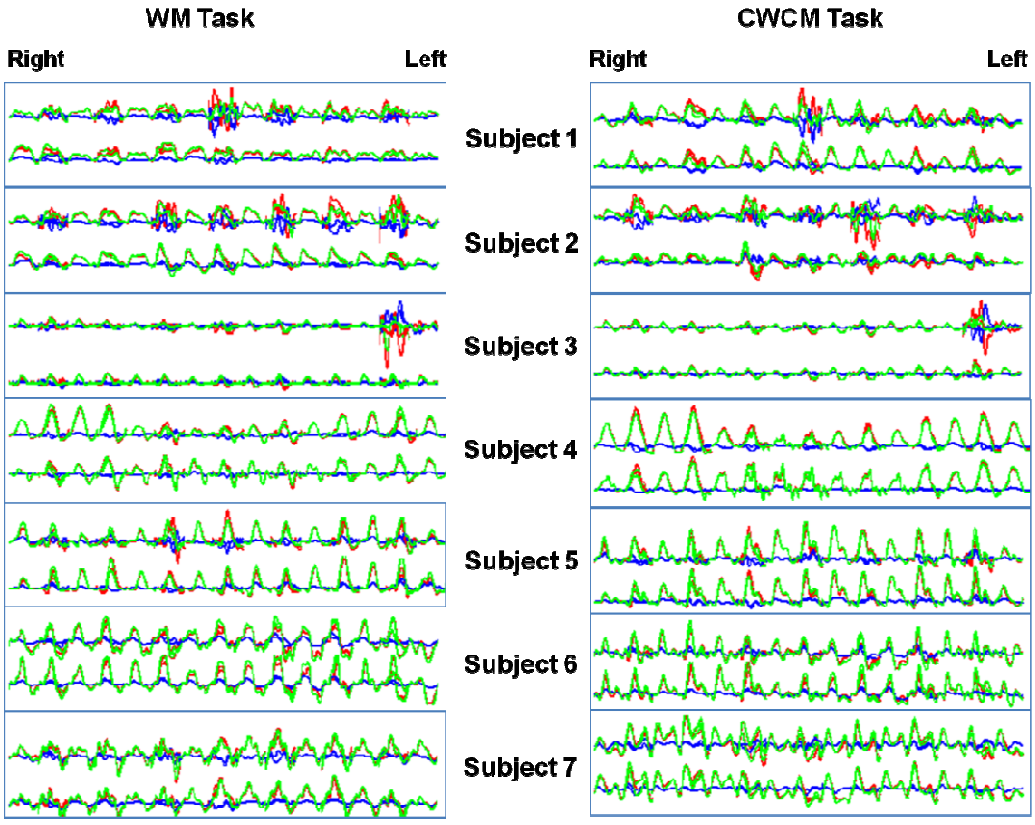

Figure 3.9 Block averaged temporal profile of HbO (green), HbR (blue) and HbT (red)

The spatial distribution of HbO concentration were calculated using a selected temporal window[26,28]. To get the spatial activation images we chose two different temporal windows. The first window is reaction period while performing the task. The first period is activation during the task, where we chose a temporal window from 0 second to the end of reaction time. The recovery period is defined as the period from response time to the end of block.

Figure 3.10 shows the activation map of HbO while performing the Stroop test. The left columns shows the activation map of all the seven subjects while performing WM task and the right shows the activation map while performing the CWCM task. The human brain template on the right corner of fig 3.9 is the representation of activation map in aPFC.

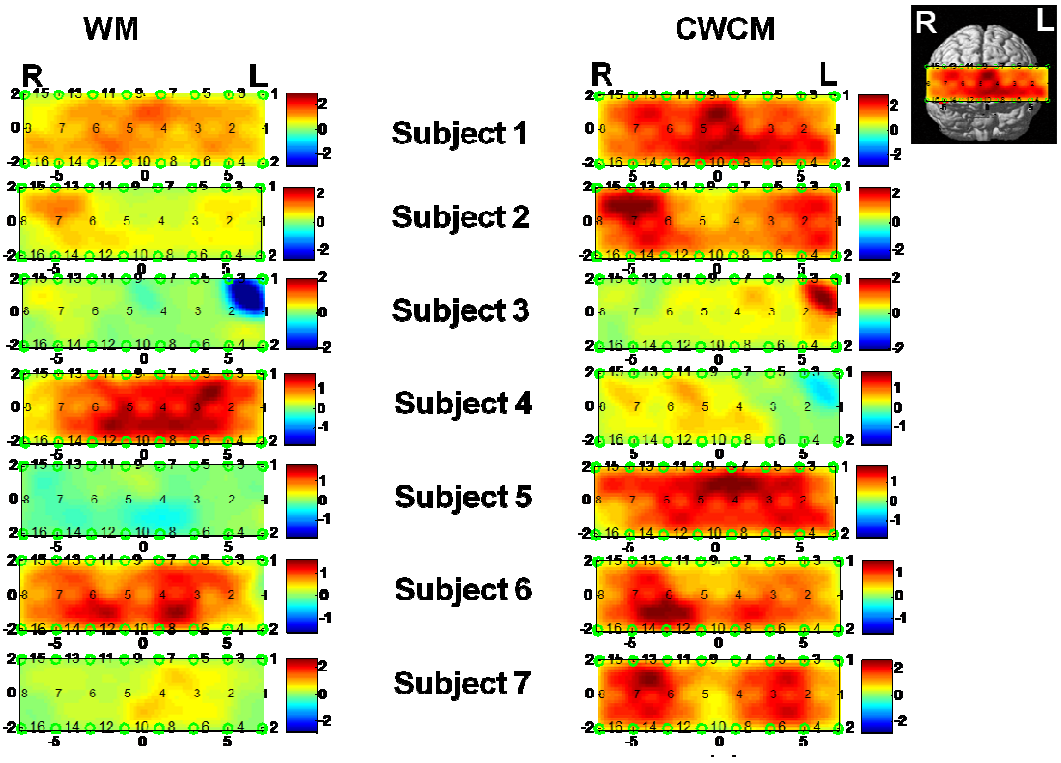

Figure 3.10 Activation map (HbO) while performing task averaged from 0 second to reaction time.

Similarly, figure 3.11 shows the activation map of HbO during recovery period. On the left corner is the activation map of recovery period while performing WM task and on right corner is the activation map of recovery period while performing CWCM task. R and L represent the right and left side of aPFC. Also, in the right corner of fig 3.10 is the representation of activation map in aPFC.

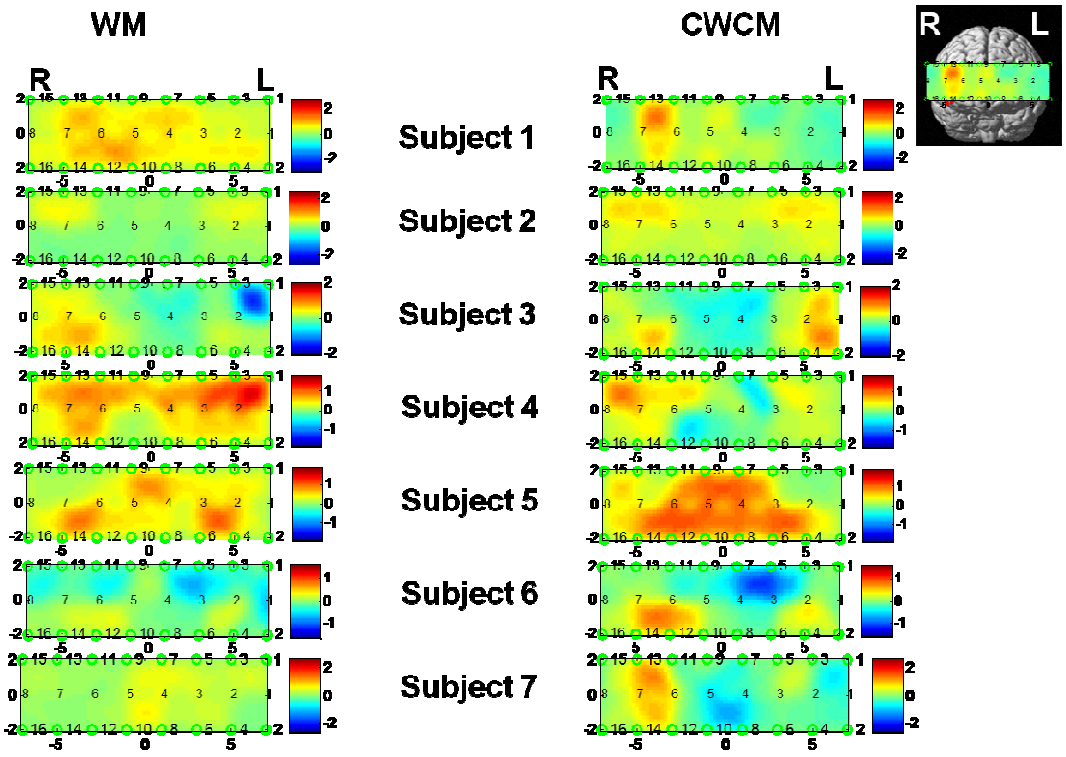

Figure 3.11 Activation map (HbO) during recovery period averaged from reaction time to end of the block.

The activation pattern of HbO during both the task is diffused throughout the aPFC. The activation pattern while performing the CWCM task is higher than while performing WM task (apart from subject 4 where the activation is higher during WM task). Also, the activation pattern of HbO was less during the recovery period than while performing the task (fig 3.10 and 3.11).

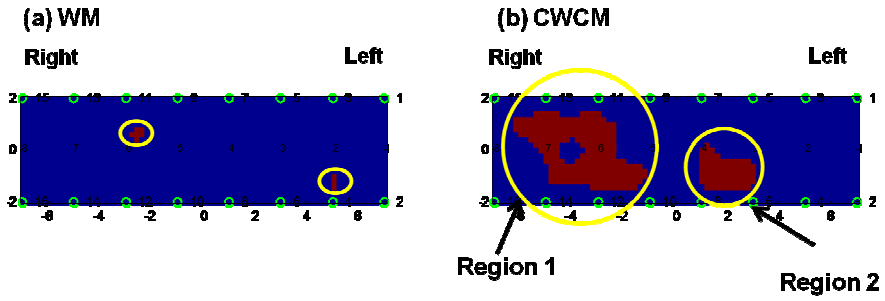

Figure 3.12 Group level t-statistics (a) WM task and (b) CWCM task. Brown region shows area of significant activation with p-value less than 0.05.

For the calculation of group level activity, a group level t-statistics was performed. A pixel-wise values of HbO changes while performing the task were taken. Pixelwise one-sample paired t-test across the subjects would determine the regions that are significantly activated from the baseline. Figure 3.12 (a) and (b) shows the regions with significant activation while performing the WM and CWCM task respectively. The brown regions in the map show the regions that are significantly activated with p-value less than 0.05. We can see that the larger regions are involved while performing CWCM task than while performing WM task. Also, larger region of right aPFC are involved while performing CWCM matching task. For further analysis we divided the regions of aPFC in region 1 and region 2 (fig 3.12). Thus we define region 1 and 2 as our region of interest.

3.3.1 Region of Interest analysis

All the pixels in the regions described above (fig 3.12 (b)) are taken into considerations for calculation. Thus, for calculation we take into account the temporal profile of each individual pixel. Then to compare and contrast between response of aPFC in two different task (WM and CWCM), we define some parameters like peak HbO (Pm) and time to peak (Tp). Pm is a single value in the temporal response where the value of HbO is maximum and Tp is the time it takes to reach Pm from beginning of the task in seconds. Figure 3.13 shows how the parameters are defined in the temporal response.

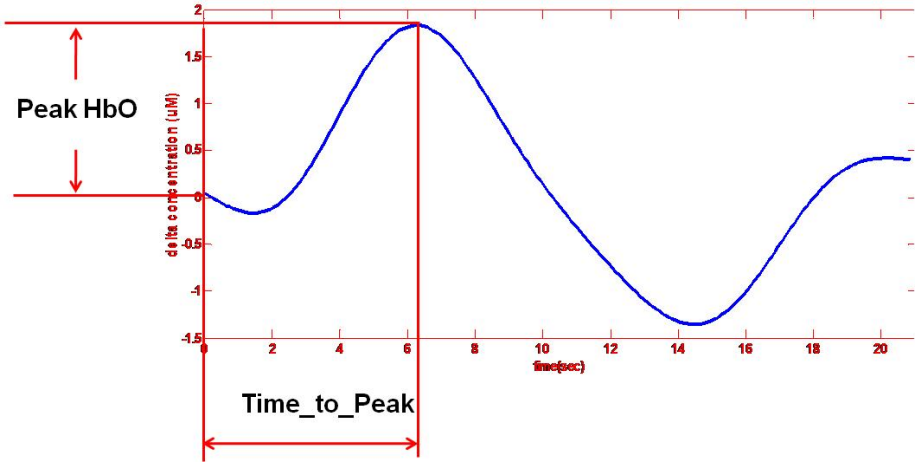

Figure 3.13 Parameters for ROI analysis.

For the analysis the values of Pm and Tp for each pixels were calculated individually. Then the response of aPFC in both task were compared in region 1 and region 2. For region 1, the mean value of Pm across all the seven subjects were 1.5±0.1 uM and 2.4±0.3 uM while performing WM task and CWCM task respectively. Similarly, the values of Tp while performing CWCM and WM task were 8.1±1.7 sec and 6.4±0.9 sec respectively. A statistical comparison between the values in two different tasks was done using repeated measures mixed model ANOVA. The p-values calculated were 0.02 and 0.4 for Pm and Tp respectively (fig 3.14(a) and (b)) which suggests that the Pm is significantly higher while performing CWCM task than performing WM task, however Pt did not show any significant difference.

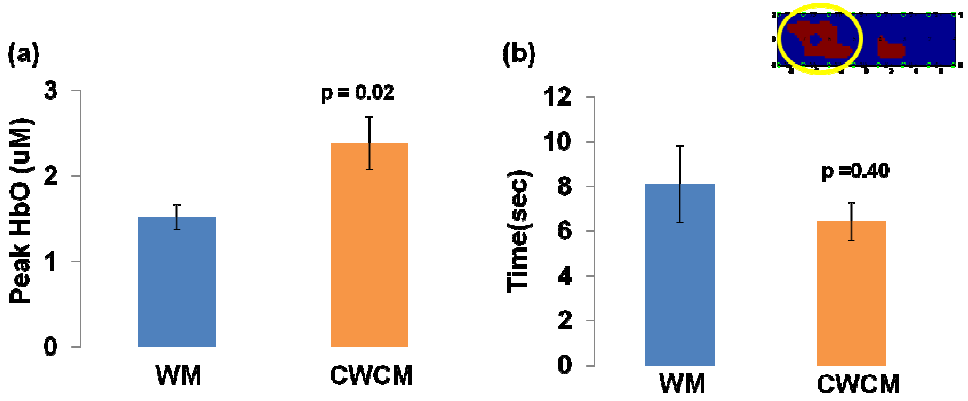

Figure 3.14 (a) Average Peak HbO and (b) Average Time to peak in region 1. Error bar in the bar diagram represents SEM.

The group average values of Pm and Tp for region 2 are shown in figure 3.15 (a) and (b) respectively. The Pm values of HbO while performing WM and CWCM task were 1.5±0.2 uM and 2.2±0.4 uM, respectively. Similarly, the Tp values were 7.9±1.9 sec and 7.6±1.4 sec, respectively. The repeated measure mixed model ANOVA on the values gives the p-value of 0.09 and 0.8 respectively for Pm and Tp. The p-values here suggest that there is no significant difference of Pm and Tp during WM and CWCM task in region 2.

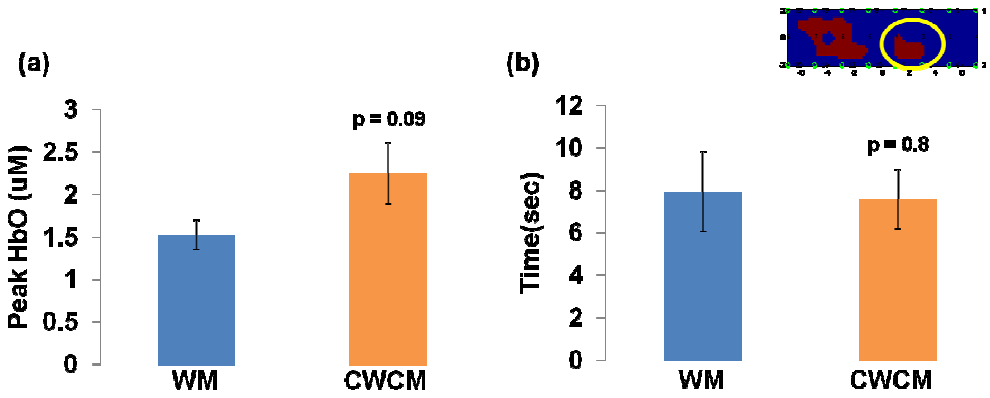

Figure 3.15 (a) Average Peak HbO and (b) Average Time to peak in region 2. Error bar in the bar diagram represents SEM.

3.3.2 Behavioral versus Hemodynamic response

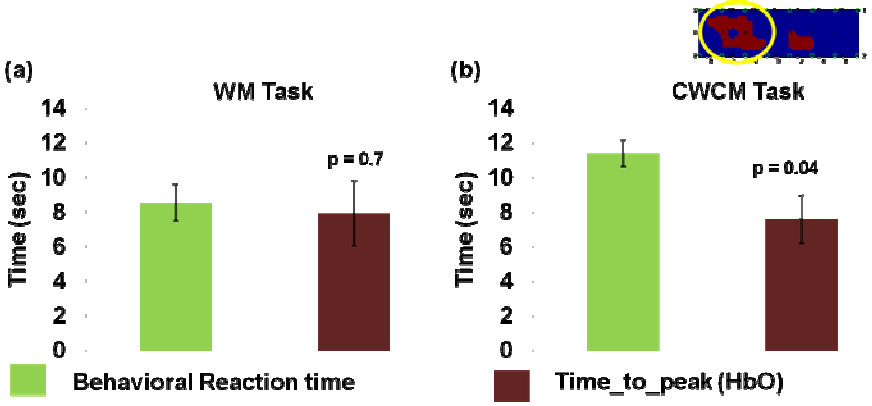

Figure 3.16 Average behavioral reaction time versus hemodynamic response while performing (a) WM task and (b) CWCM task. Error bar in the bar diagram SEM.

As mentioned above a larger area of region 1 is significantly activated while performing CWCM task than performing WM task. Furthermore from ROI analysis, region 1 demonstrated significantly higher values of Pm while performing CWCM than WM task (section 3.3.1). Thus we further analyze the data for the comparison between behavioral reaction time with hemodynamic response time viz. Tp which is discussed in the above section 3.3.1. The calculation of behavioral reaction time is discussed in detail in section 3.2.6 and that of hemodynamic response time (Tp), is discussed in detail in section3.3.1. An average value of behavioral reaction time and time to peak for each subject were calculated. For group analysis, a paired t-test across the values of each subject was carried out. The p-values between behavioral reaction time and Tp for WM task and CWCM task were found to be 0.7 and 0.04 respectively. Thus, there is no significant difference between Tp and behavioral response time while performing WM task. However, Tp was significantly less than behavioral response time while performing CWCM task suggesting HbO value reaches peak even before you complete your task.

CHAPTER 4

DISCUSSION AND CONCLUSION

4.1 Pain Study

A non-invasive fNIRS technique was used to assess a hemodynamic activity in response to the noxious pain stimuli. Using fNIRS, temporal as well as spatial response of the HbO signals in PFC were assessed.

A cluster-based analysis was performed to differentiate the temporal response of different regions in PFC. From the visual inspection of temporal response, HbO concentration shows a decrease after the pain stimuli, suggesting deactivation of HbO signal in PFC. The decrease in HbO concentration was more pronounced in moderate level of pain than in low level of pain. My initial findings were similar to some of the previous studies [44-46]. A multi-parameter analysis was done to compare and contrast the response of HbO in PFC, showing that the magnitude of HbO change was higher in response to moderate level of pain than in low level of pain. Also, change in contra-lateral side of PFC was significantly higher due to a higher level of pain stimulation, whereas there was no significant difference in ipsi-lateral side observed. A simple linear regression was performed to correlate the HbO-derived parameters and behavioral pain rating from all the subjects. From the analysis, the maximum dip of HbO and behavioral ratings showed a higher correlation coefficient (i.e., goodness of fit) in response to the moderate level of pain in medial PFC. Next, a group-level, region of interest analysis from spatial response was done. The results showed a distinct change in contra-lateral PFC in response to two different levels of pain stimuli and were similar to the cluster-based analysis.

My initial finding suggests that the contra-lateral aPFC is responsible for cognitive evaluation of pain. Also, the response of HbO in aPFC could be a potential neural correlate for cognitive evaluation of pain.

In this study, I focused my research more on the deactivation of HbO during the post-stimulus period; however, the signals in response to the pain stimulation show small increase in HbO amplitude in the initial phase. In future analysis, the study should compare this increase in amplitude as well. Also, a similar analysis of HbR and HbT response should be assessed. A large group of subjects would help in more thorough understanding, thus adding more subjects would help validate my initial findings. Also, more than two levels of pain intensity can enhance and broaden the understanding of the cognitive evaluation of pain. Furthermore, a similar study involving patients suffering from chronic pain diseases should be considered in order to compare and contrast the brain activities in cognitive perception of pain, which may help in diagnosis or monitoring of patients with chronic pain conditions.

4.2 Psychological Study

A fNIRS technique was also used to detect the hemodynamic activity in aPFC (BA 10) while performing a psychological test, namely, Stroop test. The HbO response in aPFC (BA 10) showed a detectable activity while performing the psychological test (WM and CWCM task). A visual inspection of temporal profiles of HbO changes showed a consistent increase in HbO concentration in BA 10 while performing the task. The results were consistent across all the subjects and while performing both the tasks. The spatial activation maps of HbO show that the change is higher in CWCM task than WM.

A region of interest analysis showed that a larger portion of the right aPFC is involved while performing CWCM task than performing WM task. Also, multi-parameter analysis revealed that changes in HbO are higher while performing CWCM task than performing WM task. Comparison between hemodynamic response time and behavioral reaction time showed that the time HbO signal reaches its maximum amplitude is significantly less than the behavioral reaction time for CWCM.

The initial finding from my study suggests that the aPFC is involved while performing Stroop test for cognitive functions. Also, change in concentration of HbO is higher as the task difficulty increases. Right aPFC area is involved in inhibition of Stroop interference or when more attention is required. The response of HbO in aPFC might be a potential neural correlate for human cognitive functions.

To compare and validate my initial findings, further more studies can be done. A randomized protocol between two protocols can be planned to confirm my initial findings. Similar protocols, such as Go/No-go task and flanker test, can be used to further explore cognitive functions of the brain in aPFC. Also, measurements with patients suffering from TBI (traumatic brain injury), PTSD (post-traumatic stress disorder), schizophrenia, alzheimer's disease would help researchers compare with healthy subjects and thus better understand the brain activities. Such comparison may lead to better diagnosis and treatment of those neurological disorders.

4.3 Limitations and future works:

The ROI analysis here has some limitations. Since there are many pixels in the activation map, the pixel-wise t-statistics values will result in many statistics values. Due to the large volume of values there is always the possibility of accepting the family-wise error rate, which is the likelihood that this family of pixel values could be arisen by chance (false positive results). Thus, some correction method needs to be applied to the analysis in order to avoid any values that arise just by chance. A simple and standard way of reducing or overcoming the problem is to reduce the alpha values so that the pixels are less likely to pass the significance threshold due to chance. Bonferroni correction method is a simple and stringent method in which the alpha value is decreased proportionally to the number of independent statistical test given by $\alpha_{bon} = \alpha/n$, where n is number of pixels. Thus, the Bonferroni correction effectively controls the Type I error, but also increases the probability of Type II error. Thus False discovery rate (FDR) is a more balanced technique between Type I error and Type II error [52].

To test reliability of the data, a test-retest approach could be a good method to prove and validate the method and study. Since my study had just one time measurement, test-retest operation could not be done. Thus, to test the reliability, we should repeat experiments with the same pool of subjects using the same experimental paradigm and pain level. The test-retest reliability can be done using Independent Component Analysis [53], Cluster-wise intra-class correlation coefficients [53], or channel-wise intra-class correlation coefficients (ICC) analysis [54]. The reliability and reproducibility can be tested using the above mentioned techniques.

Light traveling from the source to detector in fNIRS is diffuse, and also the source-detector separation is 3-4 cm. Thus, the spatial resolution in fNIRS is low as compared to fMRI (which is considered as gold standard in functional neuroimaging). To cross validate my results, a simultaneous fNIRS-fMRI study can be carried out using the same protocol. Thus, correlation of BOLD fMRI signal with fNIRS signals (i.e., HbO and HbR) can help us quantify and validate the spatial and temporal profiles of hemodynamic changes in response to either cognitive evaluation of pain perception or neurological/psychological tests [29, 55].

REFERENCES

[1] Boas, D. A., Dale, A. M., et al. (2004). "Diffuse optical imaging of brain activation: approaches to optimizing image sensitivity, resolution, and accuracy." Neuroimage 23: S275-S288.

[2] Gibson, A. P., Hebden, J. C., et al. (2005). "Recent advances in diffuse optical imaging." Phys. Med. Biol 50: R1-R43.

[3] Franceschini, M., Fantini S., et al. (2003). "Hemodynamic evoked response of the sensorimotor cortex measured non-invasively with the near-infrared optical imaging." Psychophysiology 40: 548-560.

[4] Near infrared imaging: Scholarpedia

[5] Schweiger, M., Gibson, A., et al. (2003). "Computational aspect of Diffuse Optical tomography." Computing in Science and Engineering 5(6).

[6] Yodh, A. and Chance, B. (1995). "Spectroscopy and imaging with diffuse light." Physics Today.

[7] Kim, J. G. and Liu, H. (2005). "Extinction coefficients of hemodynamic for near-infrared spectroscopy of tissue." IEEE Engineering in Medicine and Biology.

[8] Villringer, A. and Chance B. (1997). "Non-invasive optical spectroscopy and imaging of human brain functions." Trends in Neuroscience 20: 435-442.

[9] Yang, Y. and Raine, A. (2009). "Prefrontal structural and functional brain imaging findings in antisocial, violent, and psychopathic individuals: A meta-analysis." Psychiatry Research: Neuroimaging 174: 81-88.

[10] Miller, E. K. and Cohen, J. D. (2001). "An integrative theory of prefrontal cortex function." Annu. Rev. Neuroscience 24: 167-202.

[11] Ramnani, N. and Owen, A. M. (2004). "Anterior prefrontal cortex: insights into functions from anatomy and neuroimaging." Nature reviews 5.

[12] Bench, C. J., Frith, C. D., et al. (1993). "Investigations of the functional anatomy of attention using the Stroop test." Neuropsychologia 31(9).

[13] Fan, J., Flombaum, J. I., et al. (2003). "Cognitive and Brain Consequences of Conflict." Neuroimage 18: 42-57.

[14] Leung, H.-C., Gore, J. C., et al. (2005). "Differential anterior prefrontal cortex activation during the recognition stage of a spatial working memory task." Cerebral cortex 15: 1742-1749.

[15] Lauritzen, M., (2005). "Reading vascular changes in brain imaging: is dendritic calcium the key?" Nature reviews: Neuroscience 6.

[16] Kroger, J. K., Sabb, F. W., et al. (2002). "Recruitment of Anterior Dorsolateral Prefrontal Cortex in Human Reasoning: a Parametric Study of Relational Complexity." Cerebral cortex 12: 477-485.

[17] Christoff, K., Ream, J. M., et al. (2003). "Evaluating Self-Generated Information: Anterior Prefrontal Contributions to Human Cognition." Behavioral Neuroscience 117(6): 1161-1168.

[18] Kandel, E. R., Schwartz, J. H., and Jessel, T. M. "Principles of neural science." Fourth Edition

[19] Reiness, G.(2005) "Pain Perception."

[20] Bars, D. L., Gozaru, M., et al. (2001). "Animal Models of Nociception " Pharmacological reviews 53(4):597-652.

[21] CW6 user manual

[22] Kohlloffel, L. U. E., Koltzenburg, M., et al. (1991). " A novel technique for the evaluation of mechanical pain and hyperalgesia." Pain 46(1): 81-87

[23] Okamoto, M., Dan, H. H., et al. (2004). "Three-dimensional probabilistic anatomical cranio-cerebral correlation via the international 10-20 system oriented for transcranial functional brain mapping." Neuroimage 21(1): 99-111.

[24] Ye, J. C., Tak, S., et al. (2009). "NIRS-SPM: Statistical parametric mapping for near-infrared spectroscopy." Neuroimage 44: 428-447.

[25] Jang, K. E., Tak, S., et al. (2009). "Wavelet minimum description length detrending for near-infrared spectroscopy." Journal of Biomedical Optics 14(3).

[26] HoMER user guide

[27] Huppert, T. J., Diamond, S. G., et al. (2009). "HomER: a review of time-series analysis methods for near-infrared spectroscopy of the brain." Appl Opt 40(10): D280-D298.

[28] Boas, D. A., Dale, A. M., et al. (2004). "Diffuse optical imaging of brain activation: approaches to optimizing image sensitivity, resolution, and accuracy." Neuroimage 23: S275-S288.

[29] Strangman, G., Culver, J. P., et al. (2002). "A Qauntitative Comparison of Simultaneous BOLD fMRI and NIRS Recordings during Functional Brain Activation." Neuroimage 17: 719-731.

[30] Delpy, D. T., Cope, M., et al. (1988). "Estimation of optical pathlength through tissue from direct time of flight measurement." Phys. Med. Biol 33(12): 1433-1442.

[31] Zeff, B. W., White, B. R., et al. (2007). "Retinotopic mapping of adult human visual cortex with high-density diffuse optical tomography." PNAS 104: 12169-12174

[32] Stroop, J. (1935). "Studies of interference in serial verbal reactions." Journal of Experimental Psychology 18: 643-662.

[33] Peyron, R., Laurent, B., et al. (2000). "Functional imaging of brain responses to pain. A review and meta-analysis." NeurophysiolClin 30: 263-288.

[34] Head, H. and Holmes G. (1911). "Sensory disturbances from cerebral lesions." Brain 34: 102-254.

[35] Baliki, M. N., Chialvo, D. R., et al. (2006). "Chronic Pain and the Emotional Brain: Specific Brain Activity Associated with Spontaneous Fluctuations of Intensity of Chronic Back Pain." The Journal of Neuroscience 26(47): 12165-12173.

[36] Feist, G., Rosenberg, E., (2009) "Psychology: Making connections"

[37] MacLeod, C. M. and MacDonald, P. A., (2000). "Interdimensional interference in the Stroop effect: uncovering the cognitive and neural anatomy of attention." Trends in Neuroscience 4(10).

[38] Filosa, J. A. and V. M. Blanco (2007). "Neurovascular coupling in the mammalian brain." Experimental Physiology 92(4): 641-646.

[39] http://www.scholarpedia.org/article/Neurovascular_coupling

[40] http://www.kollewin.com/blog/electromagnetic-spectrum/

[41] http://hera.physik.uni-konstanz.de/research/biomedical_optics/index.htm

[42] http://www.scholarpedia.org/article/Near_infrared_imaging

[43] http://www.continuingedcourses.net

[44] Kong, J., White, N. S., et al. (2006). "Using fMRI to Dissociate Sensory Encoding from Cognitive Evaluation of Heat Pain Intensity." Human Brain Mapping 27: 715-721.

[45] Krishnamurthy, V., Kavuri, V., et al. (2010). "Detectability of Hemodynamic Response to Thermal Pain in Pre-Frontal Cortex Using Diffuse Optical Tomography." OSA Conference.

[46] Krishnamurthy, V. and Liu, H., (2010). "Quantified Oxy-Hemoglobin Concentration Changes in Anterior Pre-Frontal Cortex Reflecting Cognitive Evaluation of Pain Intensity using fNIRS." fNIRS Conference.

[47] Kong, J., Loggia, M.L., et al. (2010). "Exploring Brain in pain: activations, deactivations and their relation." Pain 148(2).

[48] Buckner, R.L., Andrews_Hanna, J.R., et al. (2008). "The Brain's Default Network Anatomy, Function, and Relevance to Disease." Annual New York Academy of Sciences 1124:1-38.

[49] McKiernan, K. A., Kaufman, N., et al. (2003). "A Parametric Manipulation of Factors Affecting Task-induced Deactivation in Functional Neuroimaging." Journal of Neuroscience 15(3): 394-408.

[50] Goldberg, L.L., Harel, M., et al. (2006). "When the Brain Loses its Self: Prefrontal Inactivation during Sensorimotor Processing." Neuron 50:329-339.

[51] Yan, C., Liu, D., et al. (2009). "Spontaneous Brain Activity in the Default Mode Network is Sensitive to Different Resting-State Conditions with Limited Cognitive Load." PLoS ONE 4(5).

[52] Genovese, C.R., Lazar, N.A., et al. (2002). "Thresholding of statistical maps in functional neuroimaging using the false detection discovery rate." Neuroimage 15(4):870-878.

[53] Zhang, H., Duan. L., et al., (2010). "Test-retest assessment of independent component analysis-derived resting functional connectivity based on functional near-infrared spectroscopy." Neuroimage

[54] Plichta, M.M., Herrmann M.J., et al. (2006). "Event-Related Functional Near-Infrared Spectroscopy (fNIRS) Based on Craniocerebral Correlations: Reproducibility of Activation?" Human Brain Mapping 28:733-741

[55] Huppert, T.J., Hoge, R.D., et al. (2005). "A spatial-temporal comparison of fMRI and NIRS hemodynamic responses to motor stimuli in adult humans." Proc. SPIE 5693

[56] http://hegelperuenglish.blogspot.com

[57] Cephalogics user manual.

[58] www.ergonomics.about.com

[59] Merskey, H., and Bogduk, N. “Descriptions of Chronic Pain Syndromes and Definitions of Pain Terms.” Second edition page 209-213

BIOGRAPHICAL INFORMATION

Sabin Khadka was born on January 24, 1985 in Kathmandu, Nepal. He received his Bachelor's of Engineering in Electronics and Communication Engineering from Tribhuvan University in December of 2006. In fall of 2008,he joined graduate studies from the joint program in Biomedical Engineering at University of Texas at Arlington and University of Texas Southwestern Medical Center at Dallas. Involved with multiple projects during his research, he has gained experience in the areas of neuroimaging and signal processing. He plans to join a medical device industry and extend his knowledge towards industrial projects.